Supporting Information for:

Redox, Transmetalation, and Stacking Properties of Tetrathiafulvalene-2,3,6,7-tetrathiolate Bridged Tin, Nickel, and Palladium Compounds

Jiaze Xie, Jan-Niklas Boyn, Alexander S. Filatov, Andrew J. McNeece, David A. Mazziotti and John S. Anderson*

Department of Chemistry and The James Franck Institute, University of Chicago, Chicago, Illinois 60637, United States

Correspondence to: jsanderson@uchicago.edu

Contents

General Methods

All manipulations were performed under an inert atmosphere of dry N_2 using a Schlenk line or MBraun UNIlab glovebox unless otherwise noted. Elemental analyses (C, H, N) were performed by Midwest Microlabs. Acetone was sparged with N_2 and stored in the glovebox over 4 Å molecular sieves. MeOH was dried with NaOH overnight, distilled, transferred into the glovebox and stored over 4 Å molecular sieves. All other solvents used in molecular synthesis were initially dried and purged with N_2 on a solvent purification system from Pure Process Technology. THF was further stirred with liquid NaK alloy and then filtered through activated alumina and stored over 4 Å molecular sieves. Other solvents were passed through activated alumina and stored over 4 Å molecular sieves. Unless noted, all other chemicals were purchased from commercial sources and used as received. TTFttPG (PG=-C_2H_4CN),[1] dppe$NiCl_2$[2] and [Fc][BAr^F_4][3] were prepared as previously described. [Fc^{AcO}][BAr^F_4] and [Fc^{BzO}][BAr^F_4] were prepared using the same synthetic method as [Fc][BAr^F_4] but stirred at room temperature instead of boiling DCM during [BAr^F_4]$^-$ anion exchange to avoid decomposition of Fc^{AcO} or Fc^{BzO} cations. Nuclear Magnetic Resonance (NMR) spectra for ^1H, ^{13}C, ^{31}P, ^{119}Sn were recorded on either Bruker DRX-400 or AVANCE-500 spectrometers. Tetramethyltin in CD_2Cl_2 and 85% phosphoric acid were used as reference for ^{119} Sn and ^{31}P NMR spectra, respectively. Note that ^{119}Sn NMR shifts can be affected by concentration, so caution must be used in interpreting any reported shifts.[4] All experiments were performed at room temperature. Residual solvent peaks were referenced and labelled as the deuterated solvents. Electron paramagnetic resonance (EPR) spectra were recorded on a Bruker Elexsys E500 spectrometer with an Oxford ESR 900 X-band cryostat and a Bruker Cold-Edge Stinger. Spin quantitation was performed by double integration of derivative spectra and compared to a standard Cu^{II} solution. Electrochemical experiments were performed using cyclic voltammetry (CV) on a BASi Epsilon potentiostat/galvanostat. A glassy carbon working electrode, platinum wire counter electrode, and silver wire pseudoreference electrode were used for all measurements. $FeCp_2^+$/$FeCp_2$ was used as an internal reference. Infrared spectra were recorded on a Bruker Tensor II FTIR spectrometer with MCT detector operated at 77 K. Data were processed and background corrected with OPUS software (version 7.5). An additional manual correction for scattering was also applied. Samples were prepared under N_2 by grinding solid **1-10** with Nujol, placed between two KBr crystal plates, and measured in air under ambient conditions. UV-visible-NIR absorption spectra were recorded on a Shimadzu UV-3600 Plus spectrophotometer. All solutions were prepared in an N_2-filled glovebox and transferred into a 1×1 cm quartz cuvette for room-temperature measurements in sequence. The spectrum of pure DCM in the same cuvette was used for background calibration. A Hellma Analytics Excalibur Immersion Probe with a 10 mm path length (artible no. 661-202-10-S-46) was used for variable-temperature UV-vis-NIR spectroscopic measurements and the solution of **5** in DCM was transferred to a custom-made, airtight apparatus equipped with 14/20 ground glass joint, #2 size ground glass plug and #25 size threaded Teflon plug for the immersion probe to go through which was sealed with a Teflon coated O-ring. The entire apparatus was sealed inside the glovebox before connecting to the spectrophotometer. The temperature was adjusted by adding dry ice into an isopropanol bath and each temperature point was the average of reads before and after a spectroscopic scan.Solid-state magnetic measurements were carried out with a MPMS-XL Quantum Design SQUID operating at temperatures between 1.8 and 400 K and dc magnetic fields ranging from -2 to 2 T. Measurements were performed on powder samples of **5** in sealed plastic heat-shrink tubing, whose diamagnetic contribution was corrected after experiment. All measured samples were diamagnetic in the solid state. Evans method on a $CDCl_3$ solution of **5** at room temperature was used for solution phase magnetic measurements. The diffraction data were measured at 100 K on a Bruker D8 VENTURE with PHOTON 100 CMOS detector system equipped with a Mo-target micro-focus X-ray tube (λ = 0.71073 Å). Data reduction and integration were performed with the Bruker APEX3 software package (Bruker AXS, version 2015.5-2, 2015). Alternatively, data were also collected at the Advanced Photon Source of Argonne National Laboratory (beamline 15-ID-B,C,D) using X-ray radiation with a wavelength of λ=0.41328 Å at 110 K. Data were scaled and corrected for absorption effects using the multi-scan procedure as implemented in SADABS (Bruker AXS, version 2014/5, 2015, part of Bruker APEX3 software package). The structure was solved by the dual method implemented in SHELXT[5] and refined by a full-matrix least-squares procedure using OLEX23[6] software package (XL refinement program version 2014/7[7]). Suitable crystals were mounted on a cryo-loop and transferred into the cold nitrogen stream of the Bruker D8 VENTURE diffractometer. Most of the hydrogen atoms were generated by geometrical considerations and constrained to idealized geometries and allowed to ride on their carrier atoms with an isotropic displacement parameter related to the equivalent displacement parameter of their carrier atoms. Disorder was modeled with common constraints or restraints.

Synthetic Procedures

Since compounds, **3**, **5**, **6**, **8**, and **10** can be prepared via multiple approaches, the primary bulk procedure is described in detail below while other alternative ways are reported with product formation verified by NMR spectroscopic monitoring of the reactions.

Safety note: organotin compounds are toxic. Appropriate PPE, labeling, and disposal techniques must be employed.

TTFtt$(SnBu_2)_2$ (**1**)

TTFtt$(C_2H_4CN)_4$ (11 mmol, 5.9 g) and NaOMe (86.4 mmol, 4.75 g) were added into a 500 mL Schlenk flask with dry MeOH (27 mL) in a N_2-filled glovebox. The resulting suspension was stirred at room temperature overnight until all solids disappeared and a homogeneous dark red solution was observed. This solution was transferred into a sealed Schlenk flask and brought outside the glovebox. Volatiles were then removed under vacuum. Note that the higher vacuum from a Schlenk line is required to remove the volatile byproducts of the deprotection. When the solution was dried, the Schlenk flask was sealed and transferred back into the glovebox. The remaining solid was re-dissolved in MeOH (144 mL) and treated with Bu_2SnCl_2 (43.2 mmol, 13.1 g) in MeOH (36 mL). After the mixture was stirred over an additional night at room temperature, MeOH was removed again under Schlenk line vacuum. The remaining solid was extracted with DCM and filtered sequentially through Celite and silica. After flash silica chromatography with DCM or THF, all of the filtrate was collected and dried under vacuum to provide red solid. The crude solid was washed with 10 mL of cold acetone and dried under vacuum to yield **1** as a pink powder (3.5 g, yield: 41 %). Crystals were prepared by either recrystallization from boiling MeCN followed by cooling to −35 ºC or DCM/Et_2O vapor diffusion overnight at −35 ºC. Crystals suitable for single crystal XRD were selected from the MeCN recrystallization. ^{1}H NMR (400 MHz, $CDCl_3$, 298 K): δ 0.94 (3H, t, *J* = 0.94 Hz), 1.38 (2H, q, *J* = 1.38 Hz), 1.76 (4H, m, *J* = 1.75 Hz) ppm. $^{119}Sn\{^{1}H\}$ NMR (149 MHz, $CDCl_3$, 298 K): δ 220.89 ppm. $^{13}C\{^{1}H\}$ NMR (126 MHz, CD_2Cl_2, 298 K) δ 13.61, 24.89, 26.77, 28.14, 111.59, 117.89 ppm. UV-vis-NIR (DCM, nm): 328.5, 515.6. IR (Nujol, KBr plates, cm^{-1}): 2724(m), 2668(m), 1304(m), 1288(m), 1242(w), 1173(m), 1146(m), 1075(m), 1016(w), 979(m), 966(w), 936(w), 885(s), 866(m), 846(w), 773(s), 722(s), 666(m). Anal. calc. for **1**, $C_{22}H_{36}S_8Sn_2$: C 33.26%, H 4.57%, N 0%; found: purification via DCM/Et_2O vapor diffusion: C 33.24%, H 4.52%, N none; purification via MeCN recrystallization: C 32.89%, H 4.66%, N none.

[TTFtt$(SnBu_2)_2$][BAr$^F_4$] (**2**)

1 (0.03 mmol, 24 mg) was treated with [Fc][BAr$^F_4$] (0.027 mmol, 28 mg) in Et_2O (1 mL). After stirring for 10 mins, the solution was filtered through Celite and concentrated to about 0.5 mL volume. Petroleum-ether (4 mL) was added dropwise leading to the formation of a brown precipitate. The yellow petroleum-ether supernatant was decanted gently. The solid was washed with fresh petroleum-ether and dried under vacuum to provide **2** as a brown solid (35 mg, 78 %). Suitable crystals for single crystal XRD were obtained by Et_2O/petroleum-ether layered diffusion at −35 ºC for 3 days. UV-vis-NIR (DCM, nm): 384.1, 428.6, 465.4, 490.8, 591.0, 1053.7. IR (Nujol, KBr plates, cm^{-1}): 3174(m), 2728(m), 1650(m), 1608(w), 1309(s), 1276(s), 1110(bs), 1003(w), 966(w), 887(m), 848(m), 838(m), 818(w), 769(w), 741(m), 720(s), 680(m), 668(m). EPR (THF, 15K, 9.63 GHz, 6 μW): g_{eff} = 2.008. Anal. calc. for **2**, $C_{54}H_{48}BF_{24}S_8Sn_2$: C 39.13%, H 2.92%, N 0%; found: C 38.85%, H 3.03%, N 0%.

$[TTFtt(SnBu_2)_2][BAr^F{}_4]_2$ (**3**)

Compound **1** (0.03 mmol, 24 mg) was treated with $[Fc^{BzO}][BAr^F{}_4]$ (0.066 mmol, 76 mg) in THF (1 mL). After stirring for 5 mins, the dark green solution was filtered through Celite and concentrated to about 0.5 mL volume. Petroleum-ether (4 mL) was added dropwise leading to the formation of a dark green oil-like precipitate and the orange supernatant was decanted gently. The precipitate was washed with fresh petroleum-ether (2 mL) for 3 times, redissolved in THF (1 mL), and reprecipitated by adding petroleum-ether (4 mL). The petroleum-ether supernatant was removed and the solid was washed with fresh petroleum-ether 3 times and dried under vacuum. The green solid was then collected and recrystallized from THF/petroleum-ether layered diffusion at −35 ºC for 2 days to obtain **3** as dark green-brown crystals (56 mg, 74%). The resulting crystals are suitable for single crystal XRD. ^1H NMR (400 MHz, $CDCl_3$, 298 K): δ 0.94 (3H, bt), 1.42 (2H, bs), 1.77 (4H, bs), 1.98 (s, THF adduct), 3.87 (s, THF adduct), 7.52 (s, $[BAr^F{}_4]^-$), 7.72 (s, $[BAr^F{}_4]^-$) ppm. $^{119}Sn\{^1H\}$ NMR (149 MHz, $CDCl_3$, 298 K): δ −192.70 ppm. $^{13}C\{^1H\}$ NMR (126 MHz, CD_2Cl_2, 298 K) δ 13.52, 26.83, 28.07, 117.95 (m, $[BAr^F{}_4]^-$), 125.04 (q, $[BAr^F{}_4]^-$), 129.36 (q, $[BAr^F{}_4]^-$), 162.21 (q, $[BAr^F{}_4]^-$) ppm. UV-vis-NIR (DCM, nm): 469.5, 940.5. IR (Nujol, KBr plates, cm^{-1}): 2723(w), 2666(w), 1651(s), 1608(m), 1352(s), 1278(s), 1237(w), 1119(bs), 886(m), 839(m), 742(m), 721(m), 682(m), 670(m). Anal. calc. for **3•2THF**, $C_{94}H_{76}B_2F_{48}O_2S_8Sn_2$: C 42.36%, H 2.87%, N 0%; found: C 41.91%, H 3.05%, N none. Note that the ^1H NMR spectrum of crystalline **3** in $CDCl_3$ shows broad peaks and uneven splitting patterns which suggests a small amount of radical **3** may be present (Fig. S2). Similarly, the TTF peaks in the ^{13}C NMR are not visible, again likely due to exchange with some small amount of a radical species.

If the same reaction is finished in Et_2O instead of THF, then the product is dark purple throughout the workup and **3**•$2Fc^{BzO}$ is obtained as dark purple crystals from a Et_2O/petroleum ether layered diffusion at −35 ºC for 3 days (Figure S53). Transmetalation of **3**•$2Fc^{BzO}$ is also facile as judged by ^1H NMR.

Alternative method: Compound **3** can also be generated by oxidation of **2** with 1.1 equivalents of $[Fc^{BzO}][BAr^F{}_4]$ in THF and purified as described above.

$(dppeNi)_2TTFtt$ (**4**)

$dppeNiCl_2$ (0.2 mmol, 105 mg) was suspended in DCM (3 mL) and mixed with **1** (0.1 mmol, 80 mg) in DCM (3 mL) and then stirred for 15 mins. The yellow-orange precipitate was separated by centrifugation (additional THF can help the separation). The solid was washed with THF (3 mL) 3 times and dried under vacuum. **4** was obtained as an orange powder (115 mg, 93 %). IR (Nujol, KBr plates, cm^{-1}): 2724(w), 2671(w), 1305(m), 1185(w), 1159(w), 1101(m), 1073(w), 1025 (w), 996(w), 971(w), 907(m), 873(w), 820(w), 764(w), 744(m), 690(s), 649(m). Anal. calc. for **4**, $C_{58}H_{48}Ni_2P_4S_8$: C 56.05%, H 3.89%, N 0%; found: C 55.79%, H 4.11%, N none.

$[(dppeNi)_2TTFtt][BAr^F{}_4]$ (**5**)

Compound **4** (0.03 mmol, 37.2 mg) was treated with $[Fc][BAr^F{}_4]$ (0.027 mmol, 29 mg) in DCM (3 mL) and stirred for 10 mins. After filtration through Celite, the filtrate was concentrated to about 0.5 mL and slow addition of petroleum-ether (4 mL) caused a brown precipitate to form. The petroleum-ether supernatant was removed and the precipitate was washed with fresh petroleum-ether 3 times and dried under vacuum to provide **5** as a brown solid (50 mg, 88 %). Brown crystals were obtained via PhCl/petroleum-ether vapor diffusion at room temperature for one day (32 mg, 57%). ^{1}H NMR (400 MHz, $CDCl_3$, 298 K): δ 2.44 (bs, dppe), 7.51 (s, $[BAr^F{}_4]^-$), 7.61 (bs, dppe), 7.63 (bs, dppe), 7.71 (s, $[BAr^F{}_4]^-$), 8.00 (bs, dppe) ppm. UV-vis-NIR (DCM, nm): 429.9, 457.4, 491.1, 570.3, 1268.4. IR (Nujol, KBr plates, cm^{-1}): 2721(w), 2664(w), 1274(s), 1118(bs), 1098(m), 1028(w), 998(w), 968(w), 932(w), 878(m), 838(m), 817(w), 772(w), 743(m), 680(m). Evans method ($CDCl_3$, room temperature): μ_{eff} = 1.19 B.M. EPR (THF, 15K, 9.63 GHz, 0.2 µW): g_{eff} = 2.013, 2.007, 2.003. Anal. calc. for **5**, $C_{90}H_{60}BF_{24}Ni_2P_4S_8$: C 51.33%, H 2.87%, N 0%; found: C 51.64%, H 2.98%, N none.

Alternative method: Complex **5** was also prepared through the metalation of **2** with 2 equivalents of $dppeNiCl_2$ in DCM as indicated by ^{1}H NMR spectra (Figures S13 and S14).

$[(dppeNi)_2TTFtt][BAr^F{}_4]_2$ (**6**)

*To simplify the synthesis, **3** was generated in situ and used directly for the preparation of **6**.*

Compound **1** (0.01 mmol, 8 mg) was treated with $[Fc^{BzO}][BAr^F{}_4]$ (0.022 mmol, 25 mg) in Et_2O (0.5 mL). The resulting dark purple solution was added to $dppeNiCl_2$ (0.02 mmol, 11 mg) which over 3 mins resulted in the dissolution of the yellow $dppeNiCl_2$. The solution was then filtered through Celite and concentrated to about 0.5 mL volume. Petroleum-ether (4 mL) was added to the resulting dark purple solution to precipitate the product. After gently removing the orange supernatant and washing with fresh petroleum-ether several times, the purple-red powder was dried under vacuum. Compound **6** can then be obtained as purple-red crystals by PhCl/petroleum-ether vapor diffusion at room temperature for 2 days (24 mg, 81 %). ^{1}H NMR (400 MHz, $CDCl_3$, 298 K): δ 2.47 (d, dppe), 7.48 (s, $[BAr^F{}_4]^-$), 7.50-7.60(m, dppe), 7.61-7.70 (m, dppe), 7.70 (s, $[BAr^F{}_4]^-$) ppm. $^{31}P\{^1H\}$ NMR (162 MHz, $CDCl_3$, 298 K): δ 62.95 ppm. $^{13}C\{^1H\}$ NMR (126 MHz, CD_2Cl_2, 298 K) δ 27.00 (t, dppe), 117.95 (m, $[BAr^F{}_4]^-$), 125.04 (q, $[BAr^F{}_4]^-$), 126.79 (t, dppe), 129.36 (q, $[BAr^F{}_4]^-$), 130.10(t, dppe), 133.53 (s, dppe), 133.71 (t, dppe) 156.09 (s, TTFtt), 162.21 (q, $[BAr^F{}_4]^-$), 173.46 (s,TTFtt) ppm. UV-vis-NIR (DCM, nm):515.6, 1039.5. IR (Nujol, KBr plates, cm^{-1}): 2723(w), 2670(w), 2585(w), 1354 (s), 1277(s), 1119(bs), 999(w), 958(m), 878(m), 839(m), 816(w), 745(m), 682(m). Anal. calc. for **6**, $C_{122}H_{72}B_2F_{48}Ni_2P_4S_8$: C 49.35%, H 2.44%, N 0%; found: C 49.02%, H 2.69%, N none.

Alternative method 1: Complex **6** can be obtained by direct metalation of isolated **3** or **3**•$2Fc^{BzO}$ with 2 equivalents of $dppeNiCl_2$. The products were verified by ^{1}H NMR spectra (Figures S15-S19).

Alternative method 2: **6** was also prepared by oxidation of **4** with 2 equivalents $[Fc^{AcO}][BAr^F{}_4]$ or **5** with 1 equivalent $[Fc^{AcO}][BAr^F{}_4]$ in Et_2O and the purification is the same as above (Figure S20).

$(dppePd)_2TTFtt$ (**7**)

$dppePdCl_2$ (0.06 mmol, 35 mg) was partially dissolved in DCM (2 mL) and mixed with **1** (0.029 mmol, 23 mg) in DCM (2 mL) and then stirred for 15 mins. The shiny pink precipitate was separated by centrifugation. The solid was washed with DCM (3 mL) 3 times and dried under vacuum. **7** was obtained as a pink powder (38 mg, 99 %). IR (Nujol, KBr plates, cm^{-1}): 2724(w), 2671(w), 1305(m), 1185(w), 1159(w), 1101(m), 1073(w), 1025 (w), 996(w), 971(w), 894(m), 876(m), 843(w), 822(w), 766(w), 747(m), 690(s), 649(m). Anal. calc. for **7•0.5DCM**, $C_{58.5}H_{49}ClPd_2P_4S_8$: C 50.89%, H 3.58%, N 0 %; found: C 50.70%, H 3.68%, N none. Note that the combustion analysis was calculated for a half of DCM solvate since the collected product was precipitate directly from DCM and washed with DCM.

[(dppePd)$_2$TTFtt][BAr$^F{}_4$] (**8**)

Compound **1** (0.025 mmol, 20 mg) was treated with [Fc][BAr$^F{}_4$] (0.025 mmol, 27 mg) in Et$_2$O (5 mL). The resulting dark brown solution was added to dppePdCl$_2$ (0.05 mmol, 29 mg) which over 5 mins resulted in the dissolution of the pale yellow dppePdCl$_2$. After filtration through Celite, the filtrate was concentrated to about 0.5 mL and slow addition of petroleum-ether (4 mL) caused a brown precipitate to form. The petroleum-ether supernatant was removed. After being washed with fresh petroleum-ether 3 times and dried under vacuum, brown crystals were obtained via PhCl/petroleum-ether vapor diffusion at room temperature for one day (28 mg, 51 %). ^{1}H NMR (400 MHz, CDCl$_3$, 298 K): δ 2.72 (bs, dppe), 7.50 (s, [BAr$^F{}_4$]$^-$), 7.58 (bs, dppe), 7.66 (bs, dppe), 7.71 (s, [BAr$^F{}_4$]$^-$), 8.00 (bs, dppe) ppm. UV-vis-NIR (DCM, nm): 429.9, 457.4, 491.1, 570.3, 1078.1, 1271.4. IR (Nujol, KBr plates, cm^{-1}): 2721(w), 2664(w), 1274(s), 1165(w), 1118(bs), 1098(m), 1028(w), 998(w), 968(w), 932(w), 887.4(w), 878(w), 838(m), 772(w), 743(m), 684(m). EPR (THF, 10K, 9.63 GHz, 1 μW): g_{eff} = 2.013, 2.008, 2.002. Anal. calc. for **8**, $C_{90}H_{60}BF_{24}Pd_2P_4S_8$: C 49.10%, H 2.75%, N 0%; found: C 48.88%, H 2.77%, N none.

Alternative method: Compound **7** (0.006 mmol, 10 mg) was treated with [Fc][BAr$^F{}_4$] (0.057 mmol, 6 mg) in Et$_2$O (2 mL) and stirred for 10 mins. Complex **8** was then purified with the same procedure as outlined above. (Figure S21).

(dppfPd)$_2$TTFtt (**9**)

dppfPdCl$_2$ (0.06 mmol, 44 mg) was dissolved in DCM (3 mL) and mixed with **1** (0.03 mmol, 24 mg) in DCM (2 mL) and then stirred for 15 mins. The orange precipitate was separated by centrifugation. The solid was washed with DCM (3 mL) 3 times and dried under vacuum. **9** was obtained as an orange powder (46 mg, 94 %). IR (Nujol, KBr plates, cm^{-1}): 2724(w), 2671(w), 1667(m), 1301(m), 1185(w), 1165(m), 1101(m), 1087(s), 1028 (m), 996(w), 971(w), 901(m), 873(w), 820(w), 746(m), 690(s), 632(m). Anal. calc. for **9•DCM**, $C_{75}H_{58}Cl_2Pd_2P_4S_8$: C 51.92%, H 3.37%, N 0 %; found: C 51.32%, H 3.37%, N non. Note that the combustion analysis was calculated for a DCM solvate since the collected product was precipitate directly from DCM and washed with DCM.

[(dppfPd)$_2$TTFtt][BAr$^F{}_4$] (**10**)

Compound **1** (0.009 mmol, 7.2 mg) was treated with [Fc][BAr$^F{}_4$] (0.009 mmol, 9.5 mg) in Et$_2$O (2 mL). The resulting dark brown solution was added to dppfPdCl$_2$ (0.02 mmol, 15 mg) which over 5 mins resulted in the dissolution of the red dppfPdCl$_2$. After filtration through Celite, the filtrate was concentrated to about 0.5 mL and slow addition of petroleum-ether (4 mL) caused a brown precipitate to form. The petroleum-ether supernatant was removed. After being washed with fresh petroleum-ether 3 times and dried under vacuum, brown crystals were obtained via PhCl/petroleum-ether vapor diffusion at room temperature for one day (18 mg, 80 %). ^{1}H NMR (400 MHz, CDCl$_3$, 298 K): δ 4.25 (bs, dppf), 4.55 (bs, dppf), 7.28-7.35 (m, dppf), 7.52 (s, [BAr$^F{}_4$]$^-$), 7.71 (s, [BAr$^F{}_4$]$^-$) ppm. UV-vis-NIR (DCM, nm): 429.9, 457.4, 491.1, 570.3, 1342.3. IR (Nujol, KBr plates, cm^{-1}): 2721(w), 2664(w), 1667(m), 1353(s), 1274(s), 1157(m), 1118(bs), 1089(m), 1035(w), 1028(w), 998(w), 968(w), 924(w), 885(m), 838(m), 821(m), 743(m), 711(m), 692(m), 680(m), 668(m), 628(m). EPR (THF, 10K, 9.63 GHz, 0.4 μW): g_{eff} = 2.014, 2.008, 2.001. Anal. calc. for **10**, $C_{106}H_{68}BF_{24}Fe_2Pd_2P_4S_8$: C 50.66%, H 2.73%, N 0%; found: C 50.78%, H 2.86%, N none.

Alternative method: Compound **9** (0.005 mmol, 8 mg) was treated with [Fc][$BAr^F{}_4$] (0.045 mmol, 4.5 mg) in Et_2O (2 mL) and stirred for 10 mins. Complex **10** was then purified with the same procedure as outlined above. However, the product collected via the direct oxidation is typically associated with an impurity, likely **9**, although pure crystals can be grown (Figure S22).

NMR Spectra

1. ^{1}H NMR Spectra

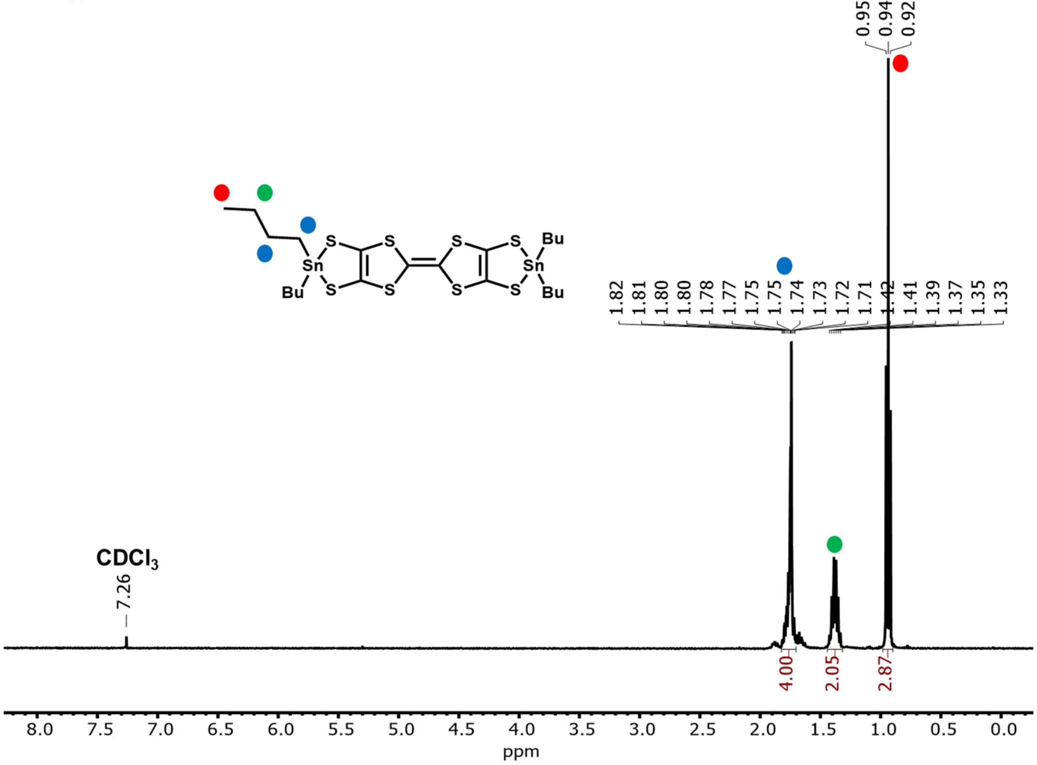

Figure S1. ^{1}H NMR spectrum of **1** in $CDCl_3$.

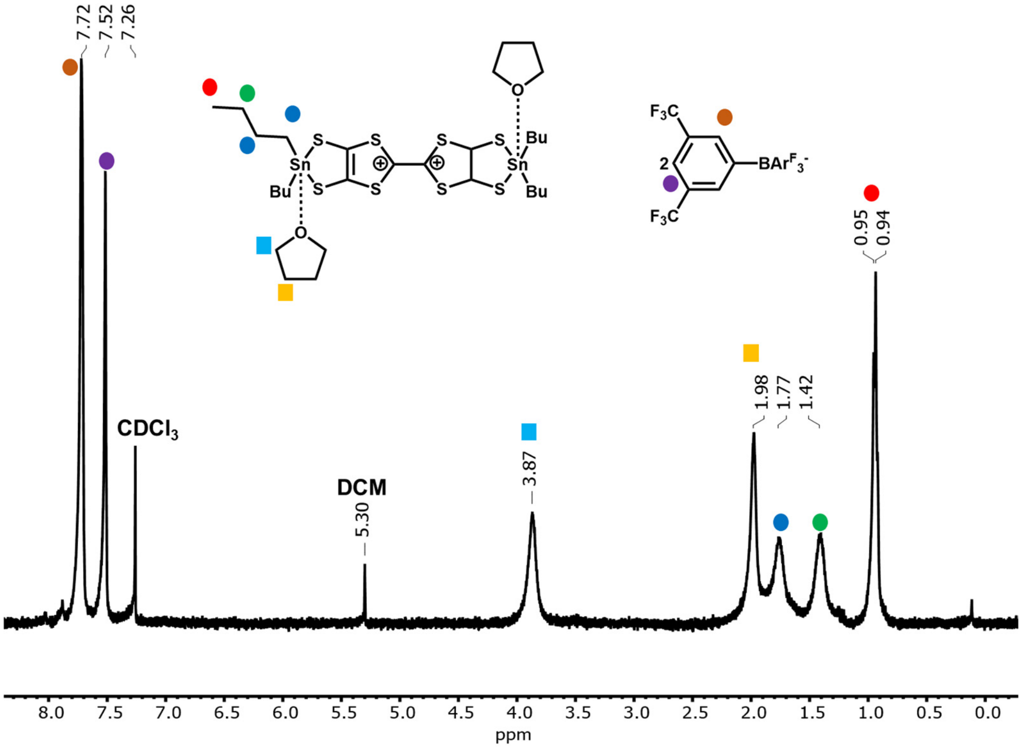

Figure S2. ^{1}H NMR spectrum of **3•2THF** in $CDCl_3$.

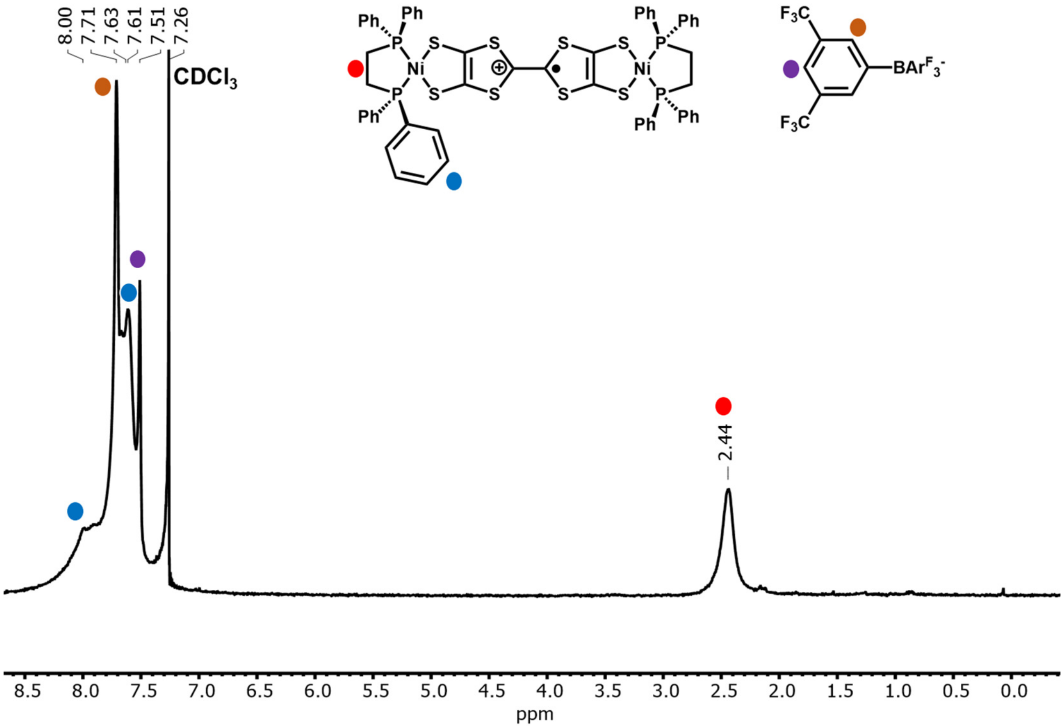

Figure S3. ^{1}H NMR spectrum of **5** in CDCl$_3$.

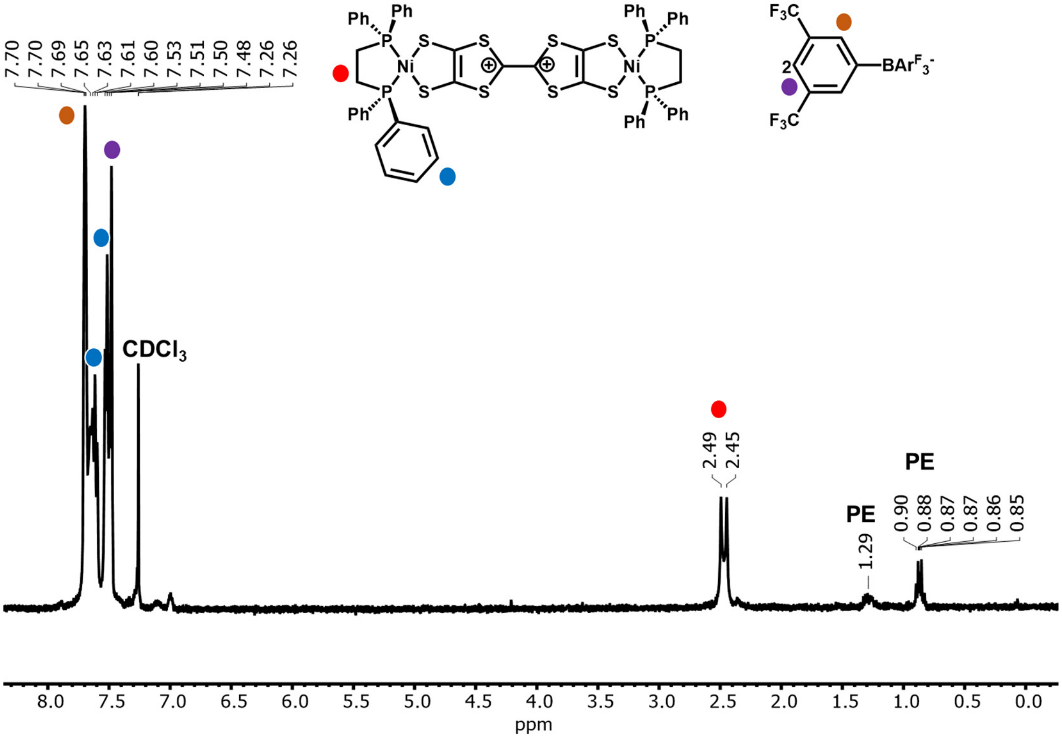

Figure S4. ^{1}H NMR spectrum of **6** in CDCl$_3$.

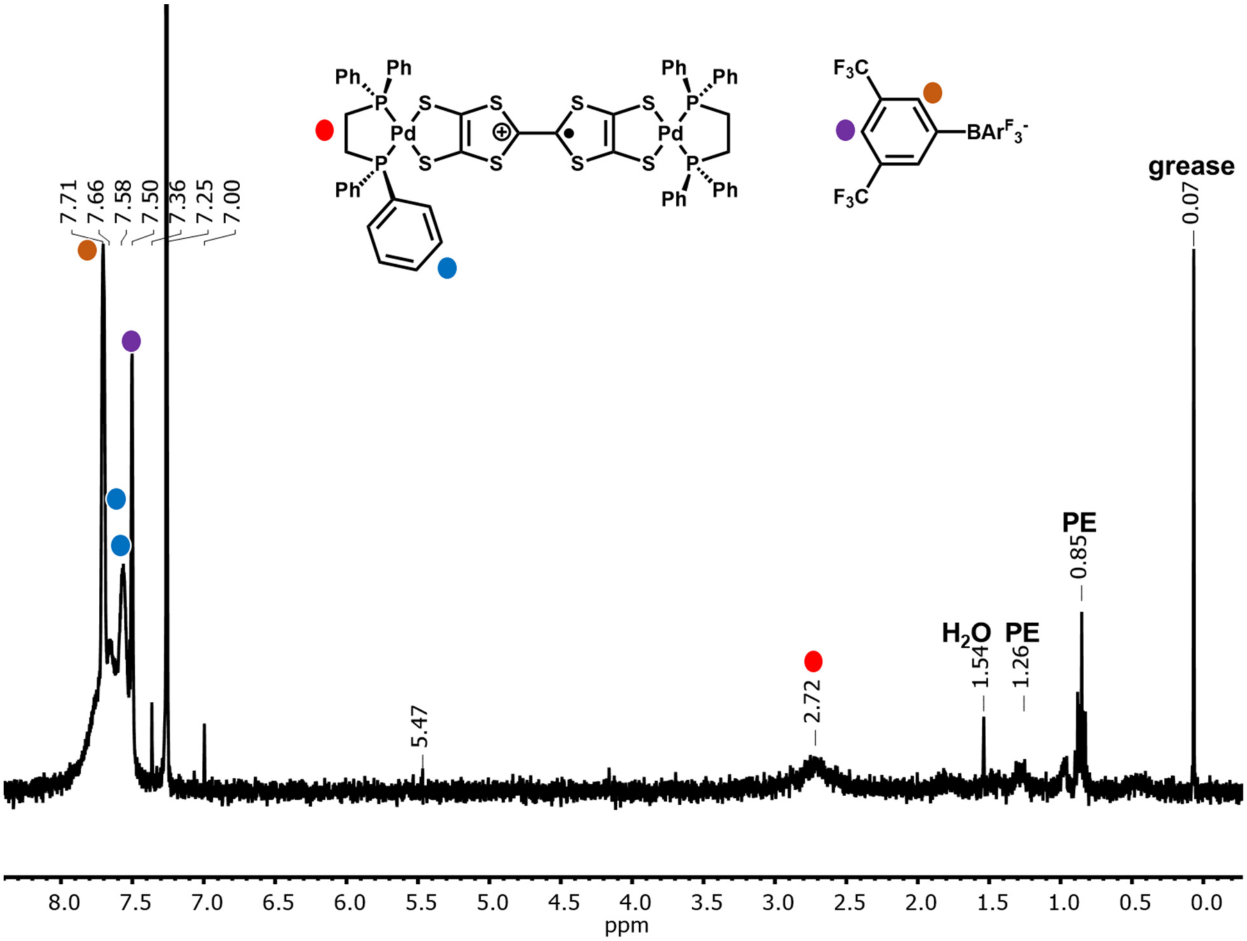

Figure S5. ^{1}H NMR spectrum of **8** in $CDCl_3$.

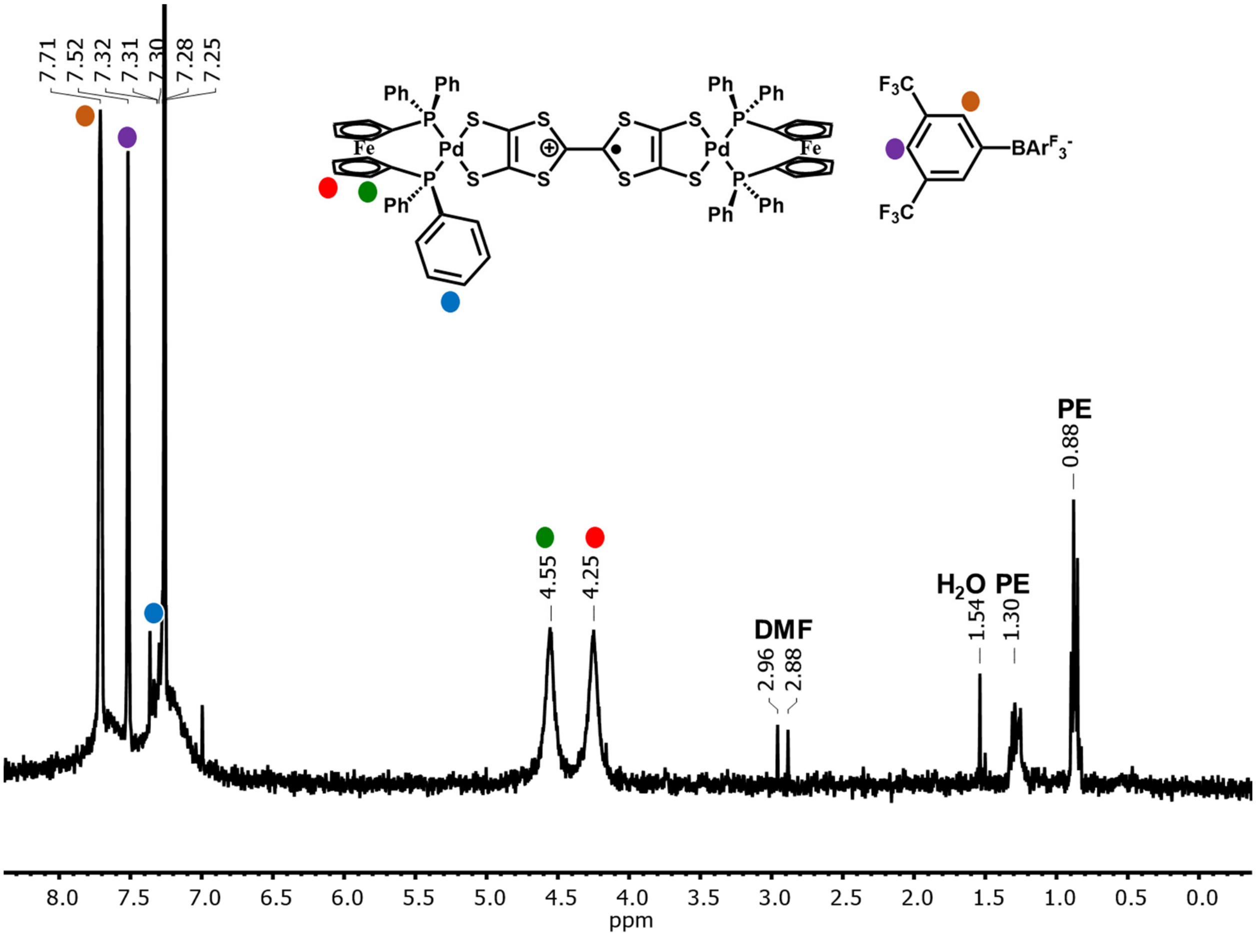

Figure S6. ^{1}H NMR spectrum of **10** in CDCl$_3$.

2. ^{13}C NMR Spectra

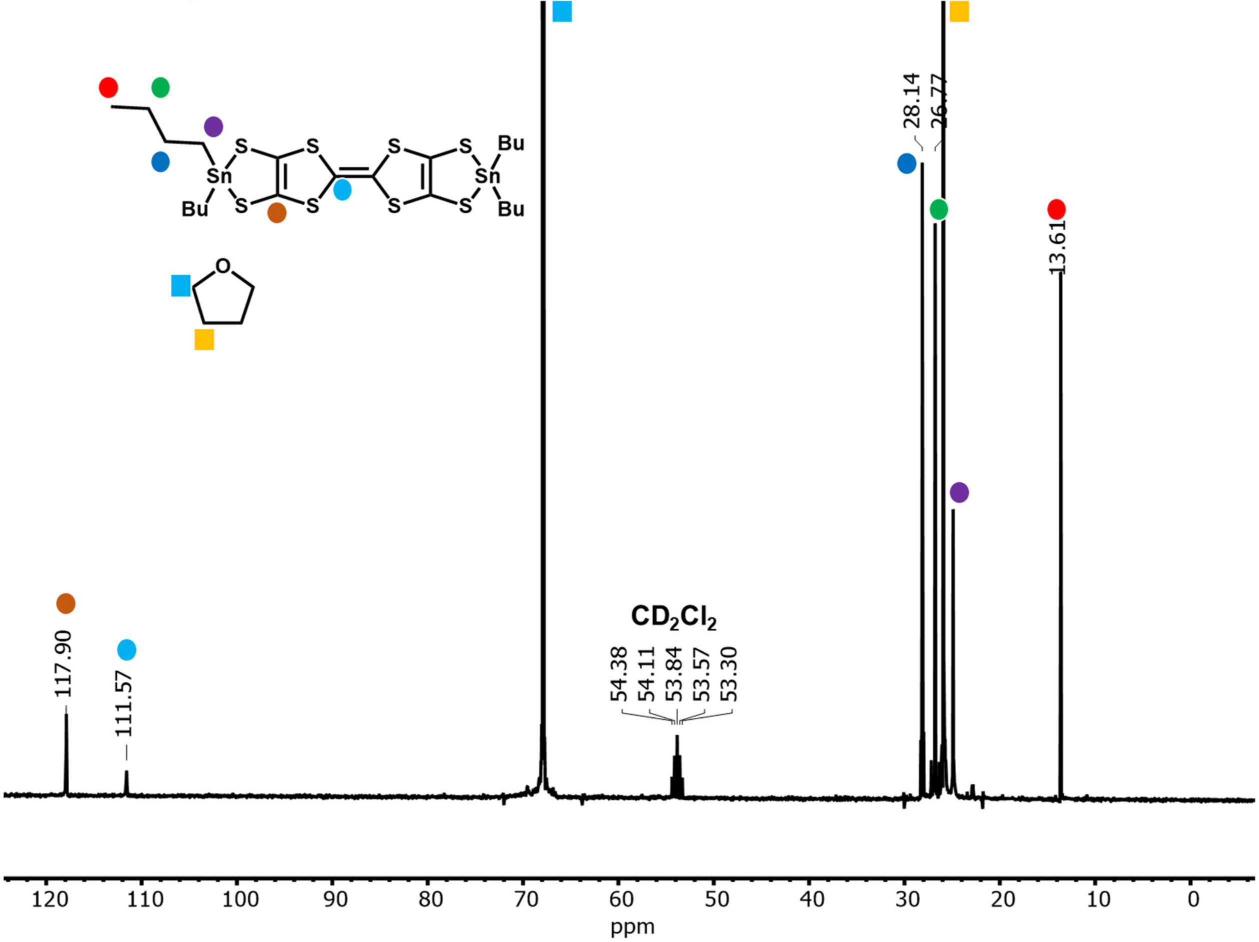

Figure S7. ^{13}C{^{1}H} NMR spectrum of **1** in 0.5 mL THF + 0.1 mL CD_2Cl_2.

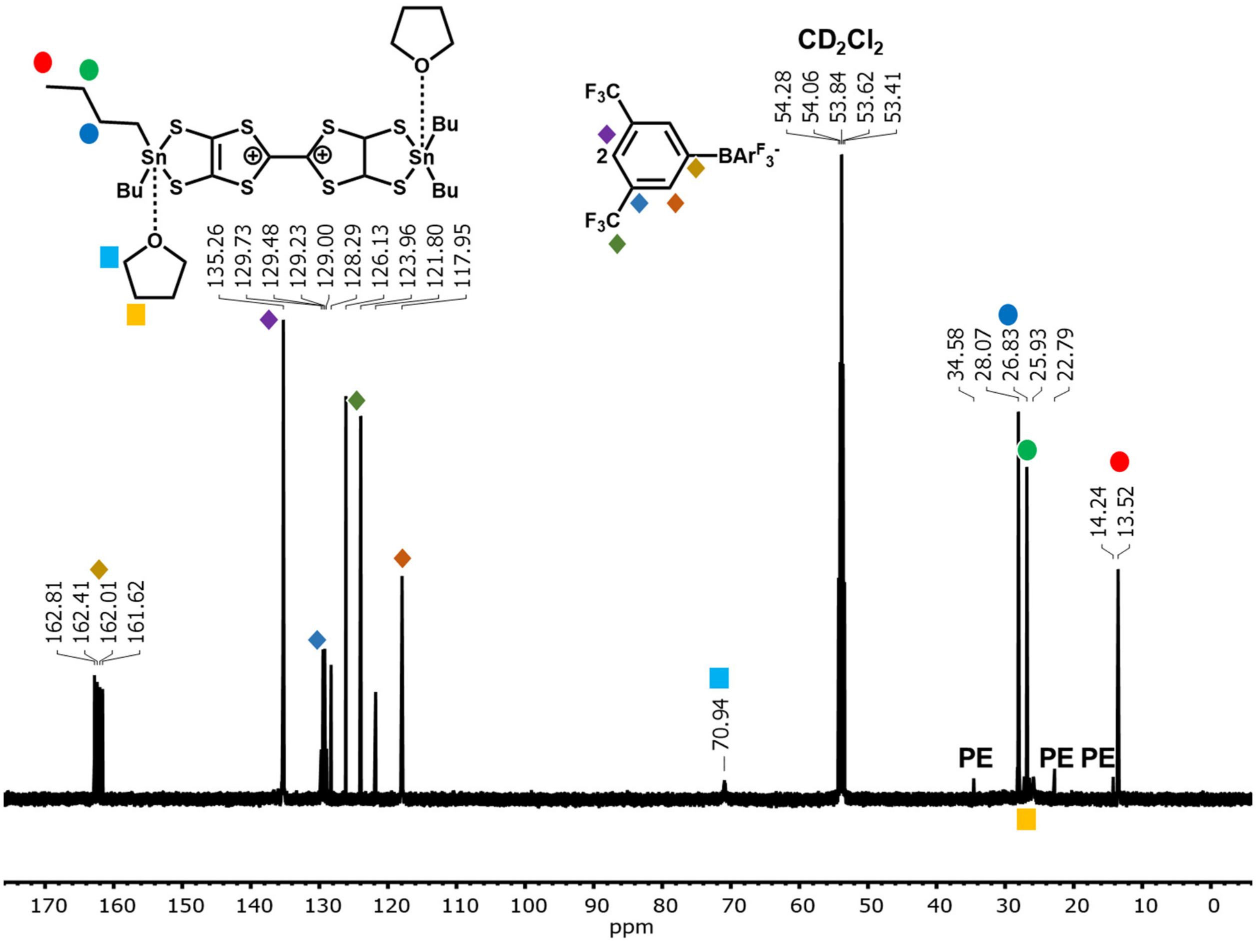

Figure S8. $^{13}C\{^1H\}$ NMR spectrum of **3** in CD_2Cl_2. Due to a possible exchange with a small amount of radicals, the peaks of TTF and the first carbon of butyl groups connecting to the Sn atoms are not visible.

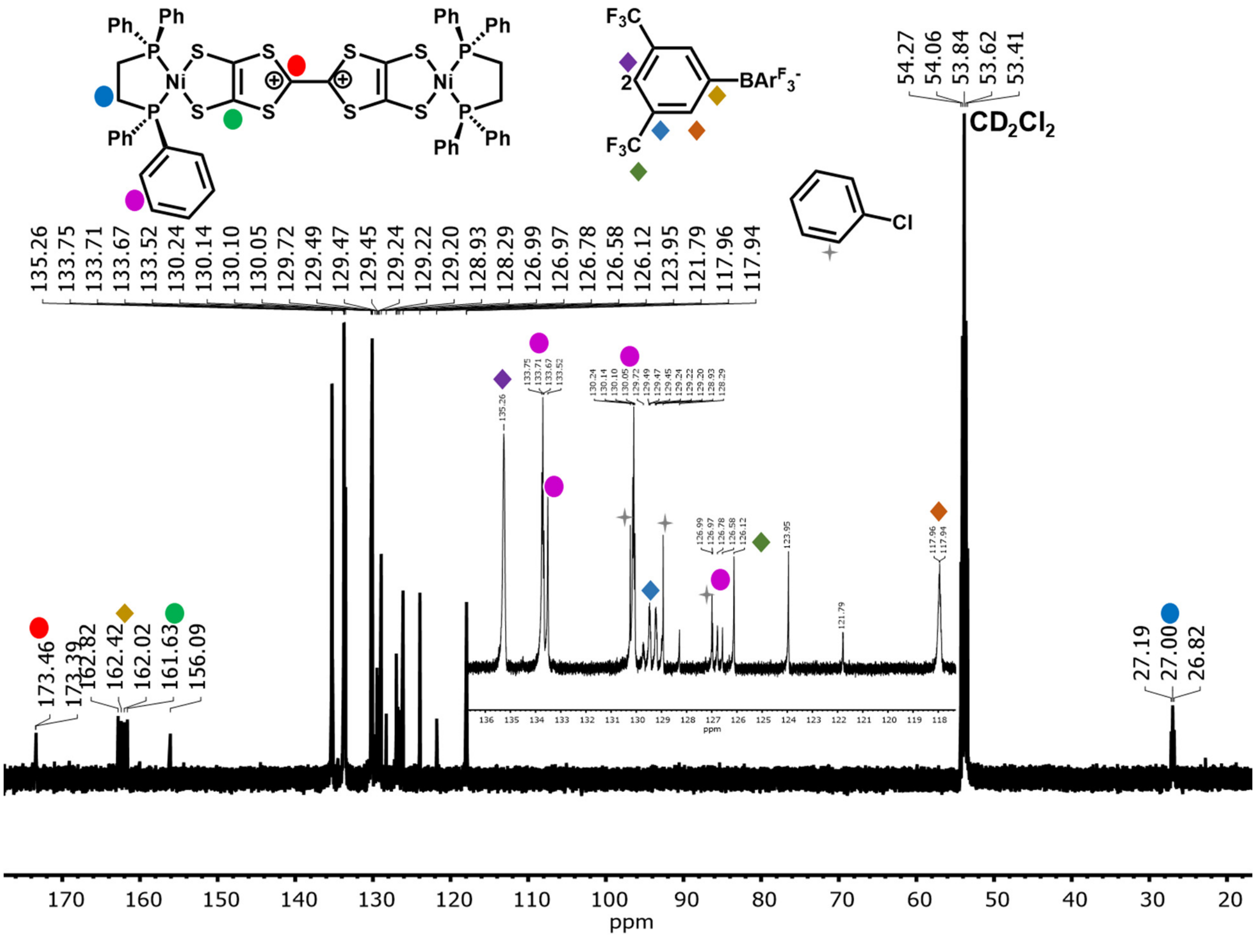

Figure S9. $^{13}C\{^1H\}$ NMR spectrum of **6** in CD_2Cl_2 **.** The spectrum from 118-136 ppm is expanded and shown in the inset graph.

3. ^{31}P NMR Spectra

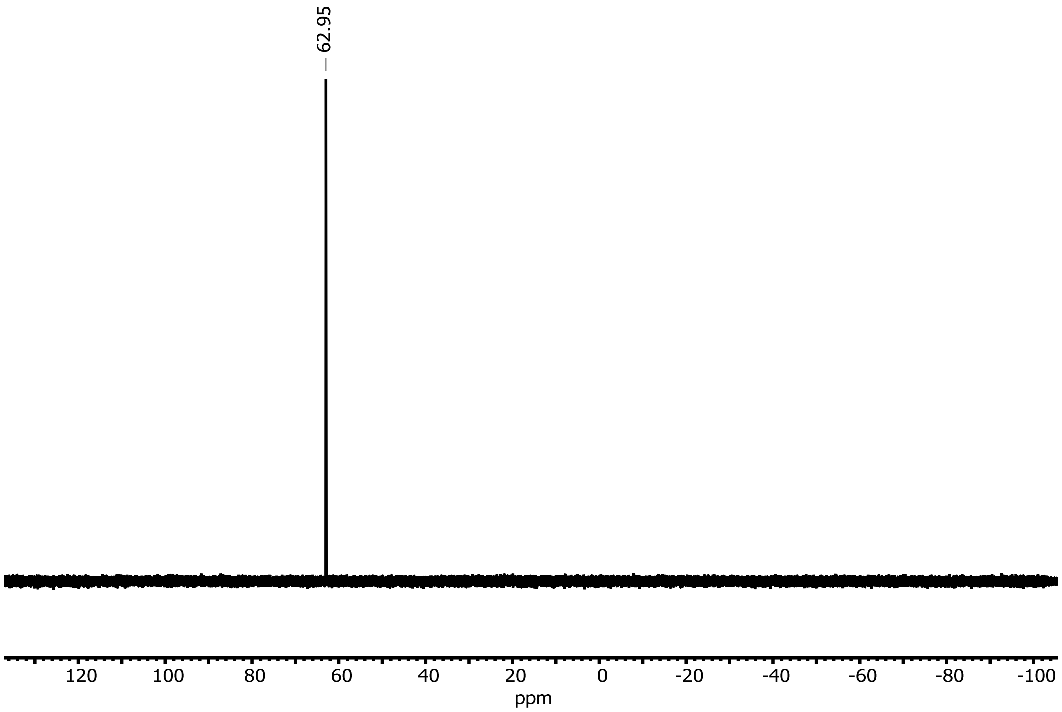

Figure S10. $^{31}P\{^1H\}$ NMR spectrum of **6** in $CDCl_3$.

4. ^{119}Sn NMR Spectra

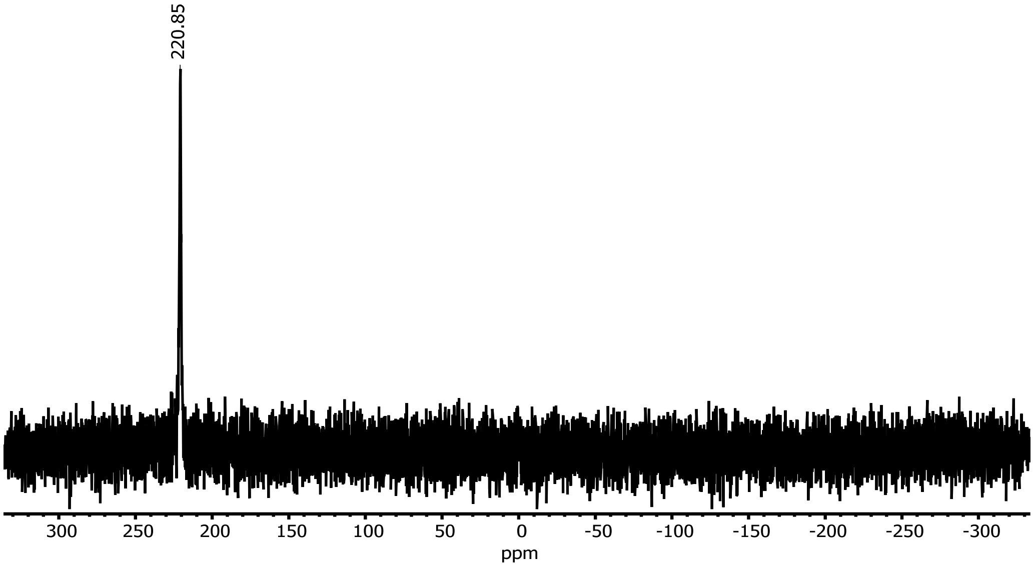

Figure S11. $^{119}Sn\{^1H\}$ NMR spectrum of **1** in $CDCl_3$.

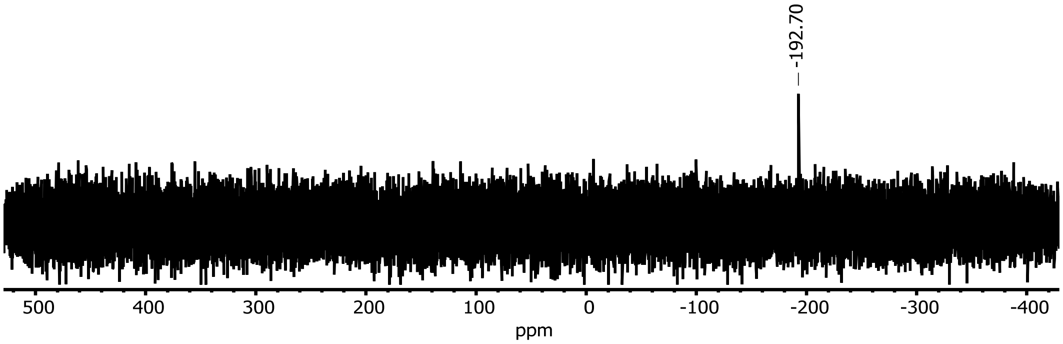

Figure S12. ^{119}Sn{^{1}H} NMR spectrum of **3** in CDCl$_3$.

Alternative synthesis methods monitored by ^{1}H NMR experiments

1. Synthesis of 5 by metalation of 2

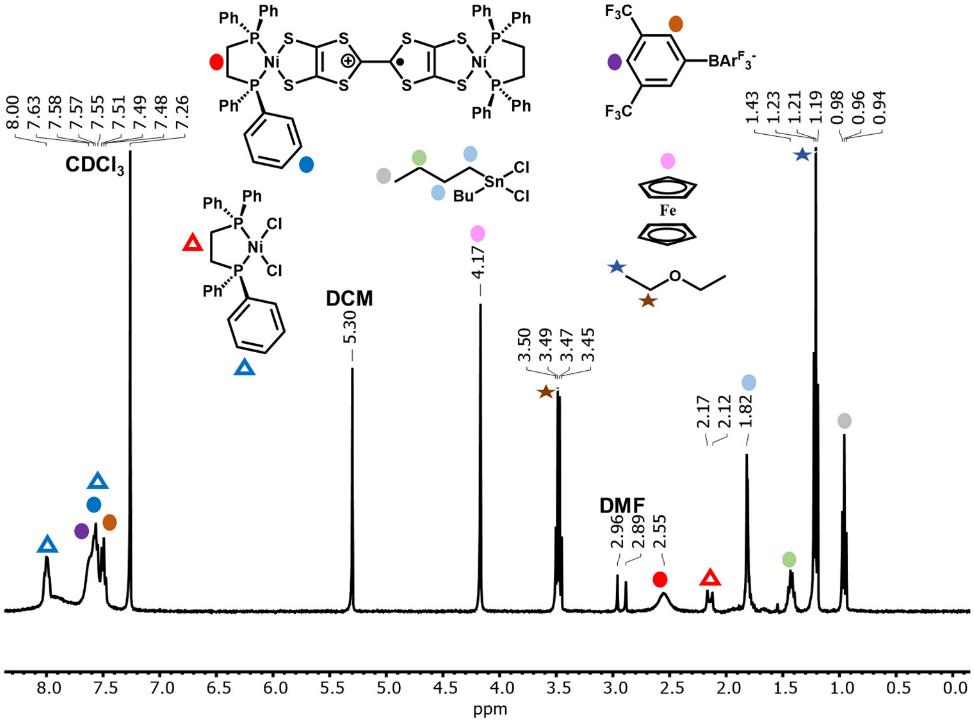

Figure S13. ^{1}H NMR spectrum in CDCl$_3$ of metalation products of **2**. Note the residual dppeNiCl$_2$ was due to an excess of this reagent added to the reaction.

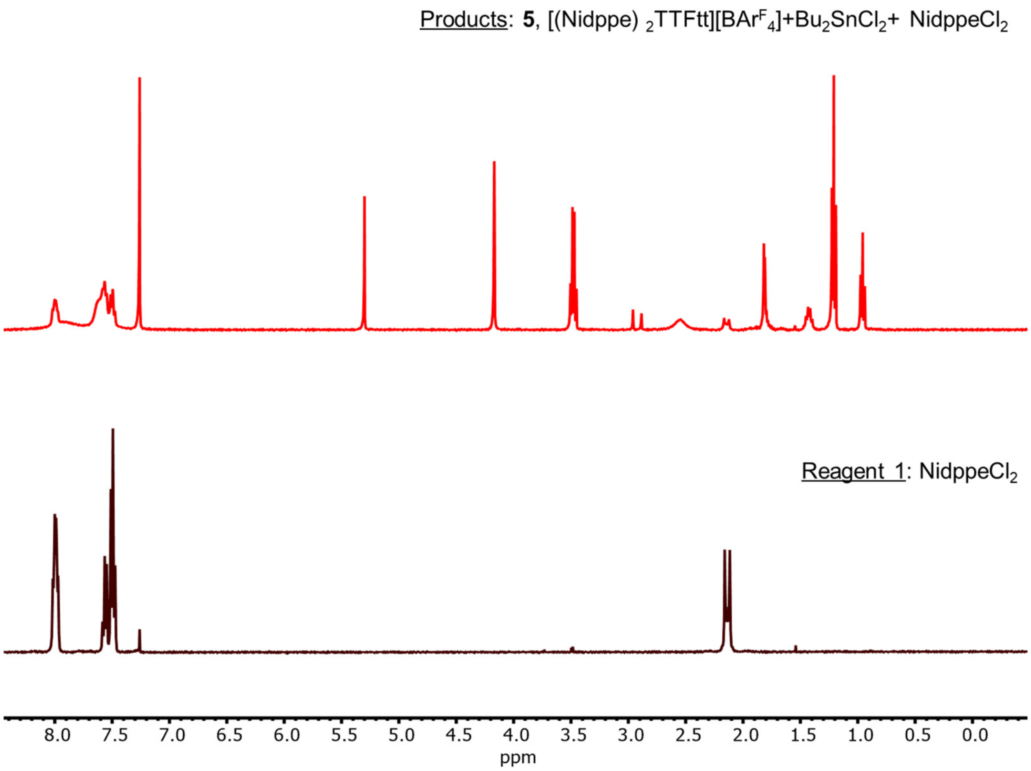

Figure S14. ^{1}H NMR spectra in $CDCl_3$ monitoring the metalation process of **2**.

2. Synthesis of 6 by metalation of 3•2THF

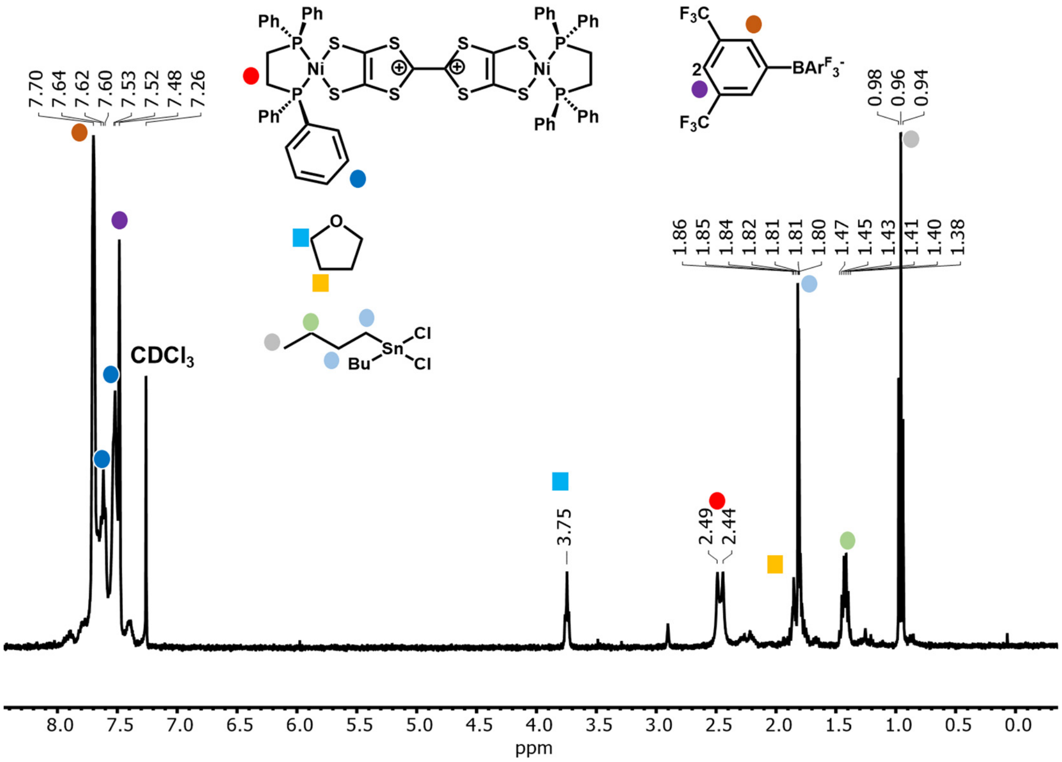

Figure S15. ^{1}H NMR spectrum in $CDCl_3$ of metalation products of **3•2THF**.

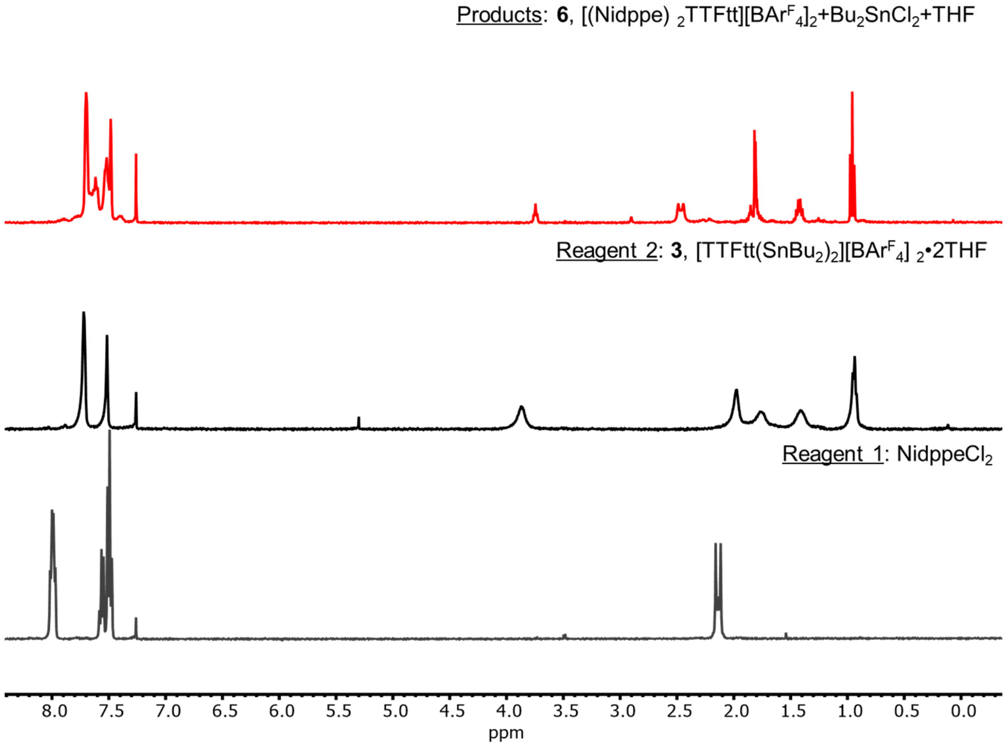

Figure S16. ^{1}H NMR spectra in CDCl$_3$ monitoring the metalation process of **3•2THF**.

3. Synthesis of 6 by metalation of 3•2Fc^{BzO}

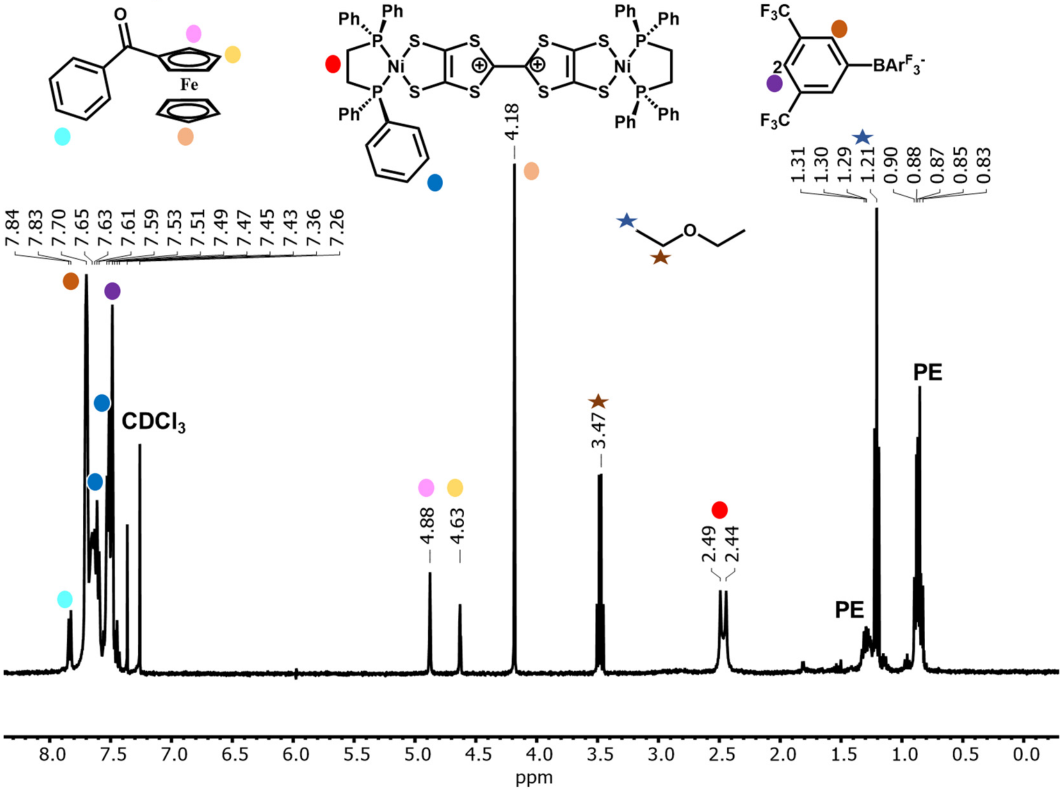

Figure S17. ^{1}H NMR spectrum in CDCl$_3$ of metalation products of **3•2Fc^{BzO}** after petroleum-ether extraction.

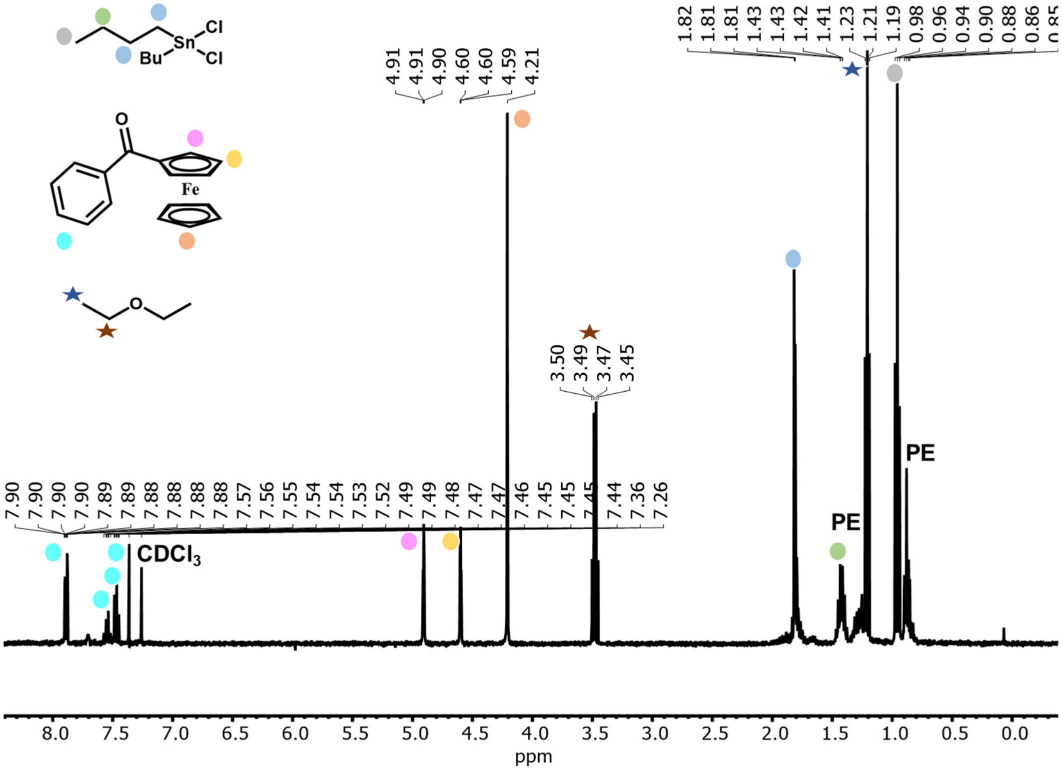

Figure S18. ^{1}H NMR spectrum in $CDCl_3$ of metalation products of **3•2Fc^{BzO}** in extracted petroleum-ether portion.

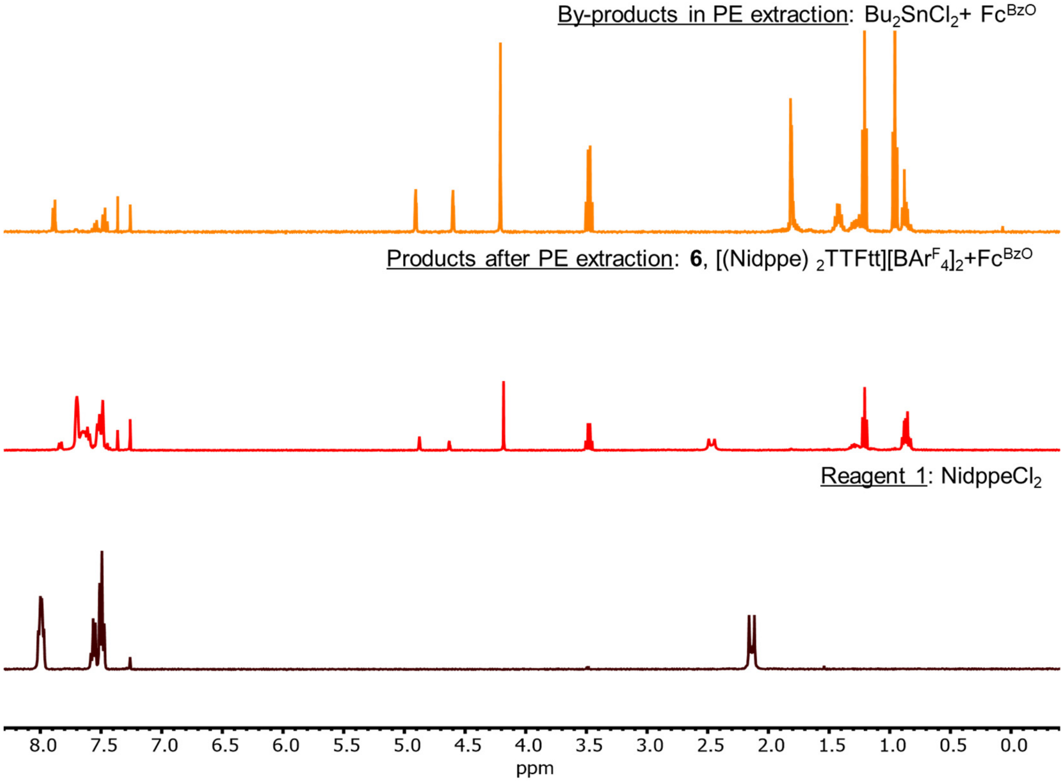

Figure S19. ^{1}H NMR spectra in $CDCl_3$ monitoring the metalation process of **3•2Fc^{BzO}**.

4. Synthesis of 6 by oxidation of 4.

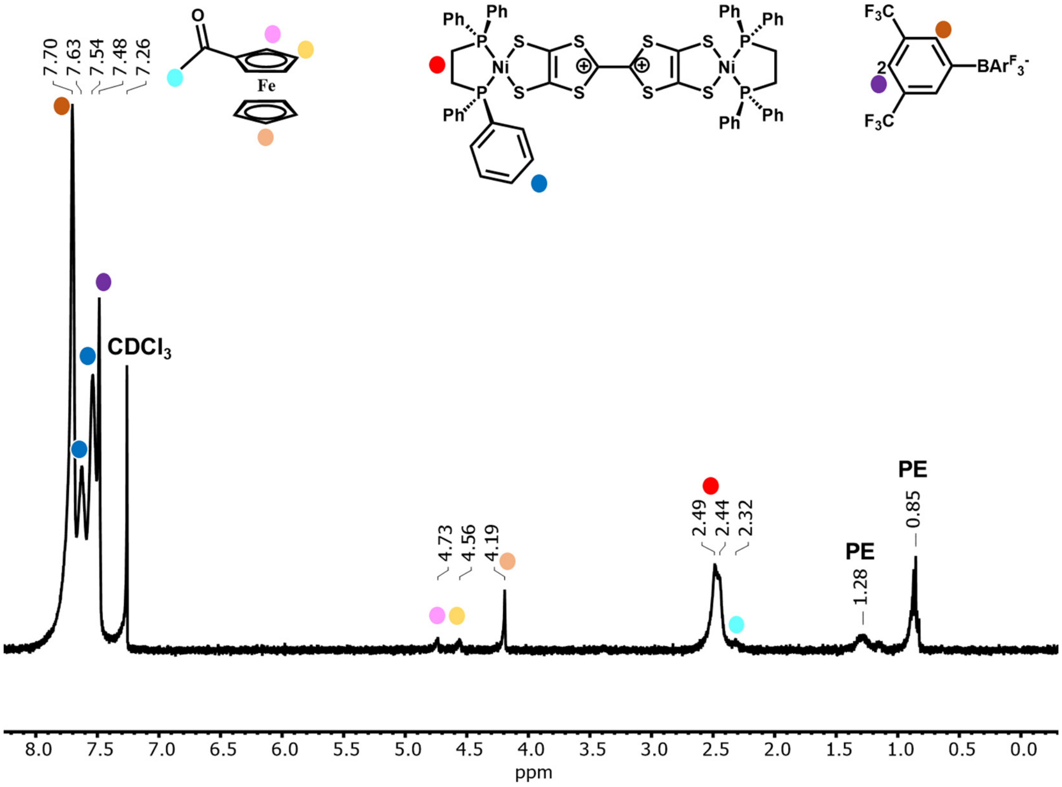

Figure S20. ^{1}H NMR spectrum in $CDCl_3$ of oxidation products of **4**.

5. Synthesis of 8 by oxidation of 7.

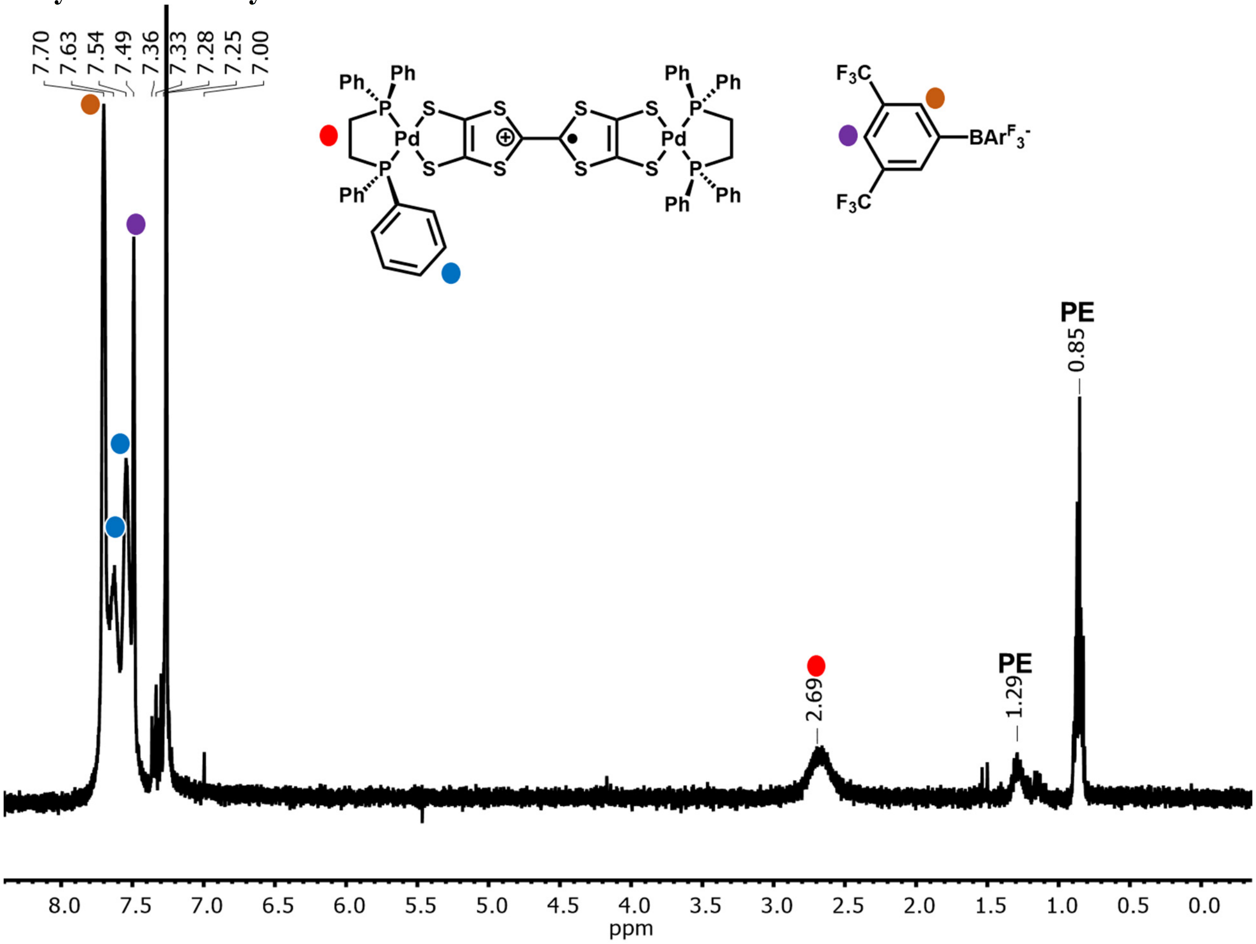

Figure S21. ^{1}H NMR spectrum in $CDCl_3$ of **8** via oxidation of **7**.

6. Synthesis of 10 by oxidation of 9.

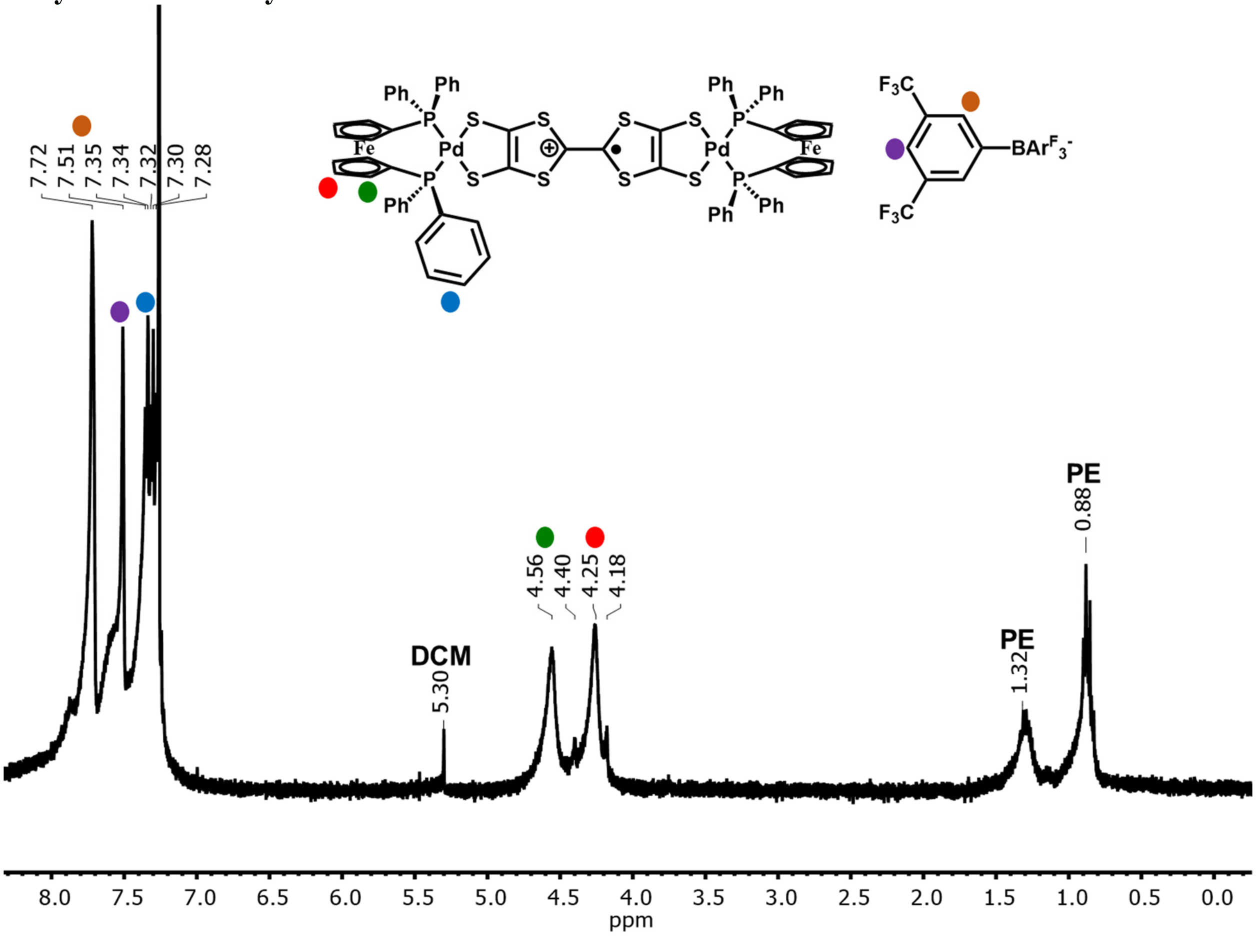

Figure S22. ^{1}H NMR spectrum in CDCl$_3$ of **10** via oxidation of **9**. Two additional peaks at 4.18 and 4.40 ppm are assigned as probably mixed **9**.

Air stability test of 6 monitored by ^{1}H and ^{31}P NMR spectra

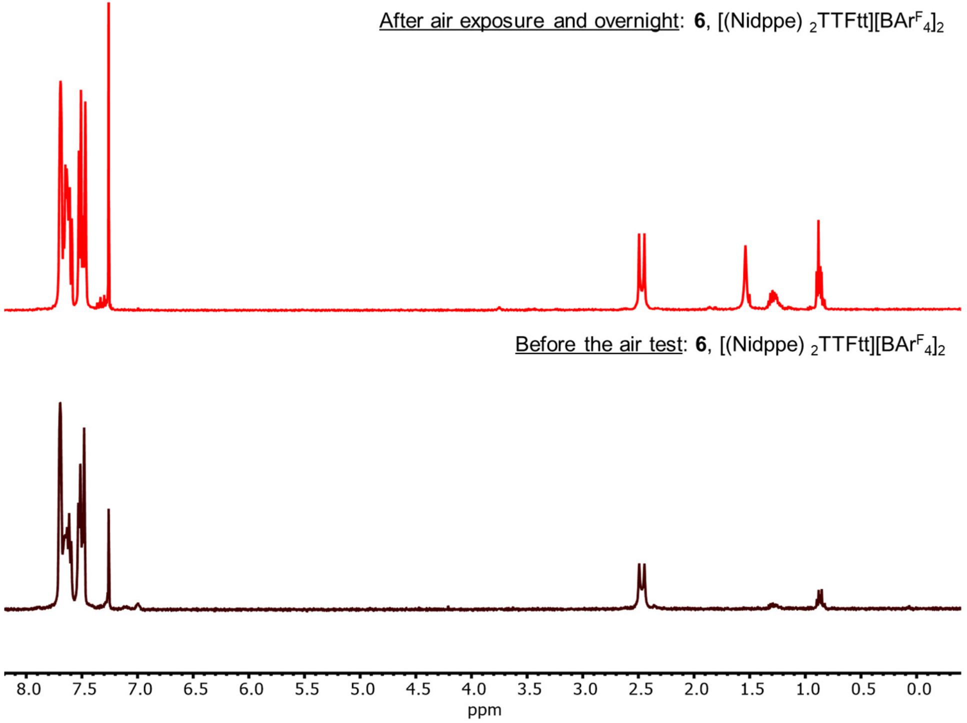

Figure S23. ^{1}H NMR spectrum of **6** in $CDCl_3$ before and after air exposure for 35 mins and sealed placement overnight.

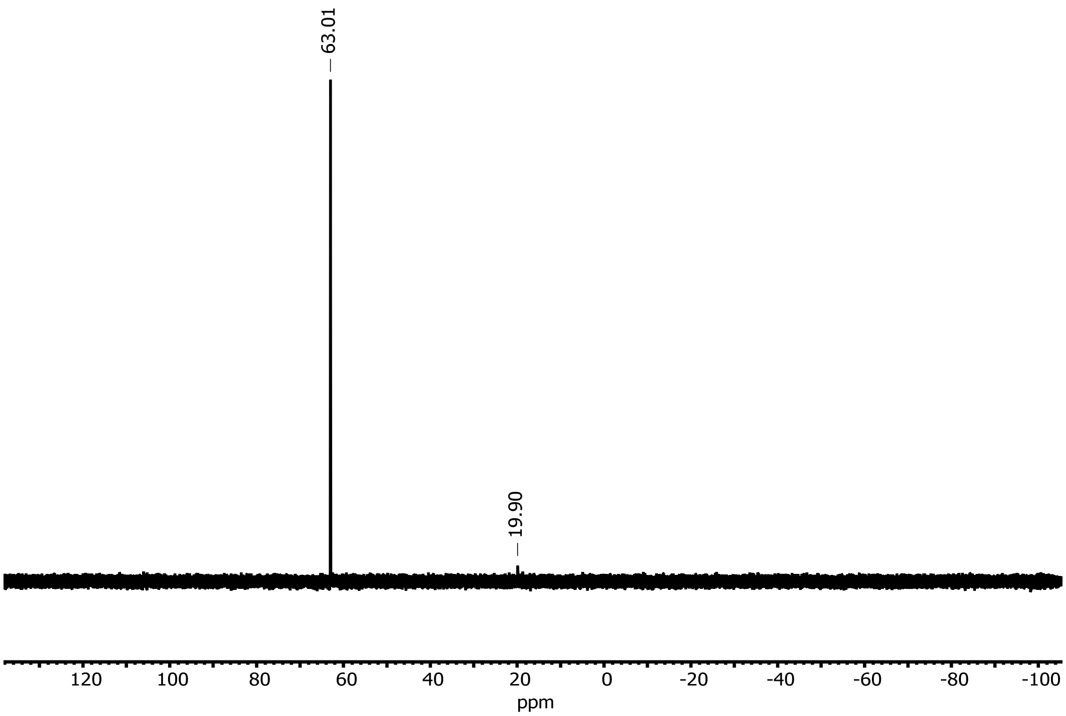

Figure S24. $^{31}P\{^{1}H\}$ NMR spectrum of **6** in $CDCl_3$ after air exposure for 35 mins and sealed placement overnight.

EPR Spectra

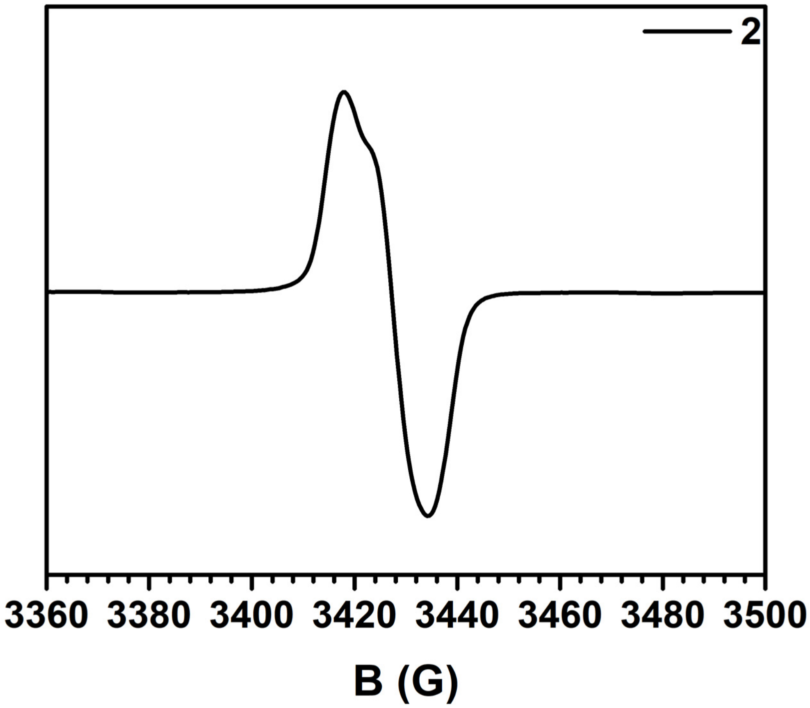

Figure S25. X-band EPR spectrum of **2** collected on a 3 mM solution in THF at 15 K.

Microwave frequency: 9.63 GHz, microwave power: 6 μW, and $g_{\text{eff}} = 2.008$.

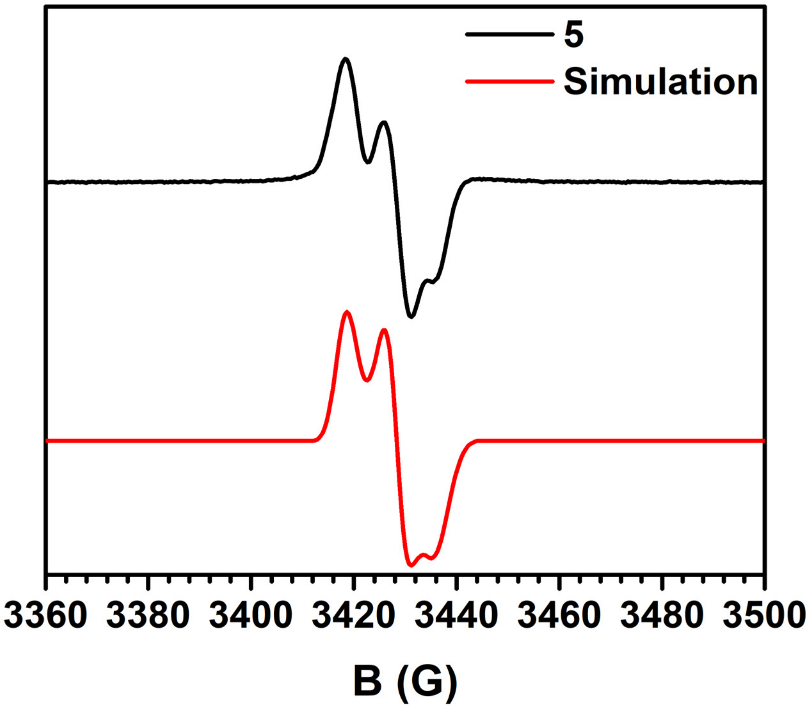

Figure S26. X-band EPR spectrum of **5** collected on a 1 mM solution in THF at 15 K. Microwave frequency: 9.63 GHz, microwave power: 0.2 μW, and $g_{\text{eff}} = 2.013, 2.007, 2.003$.

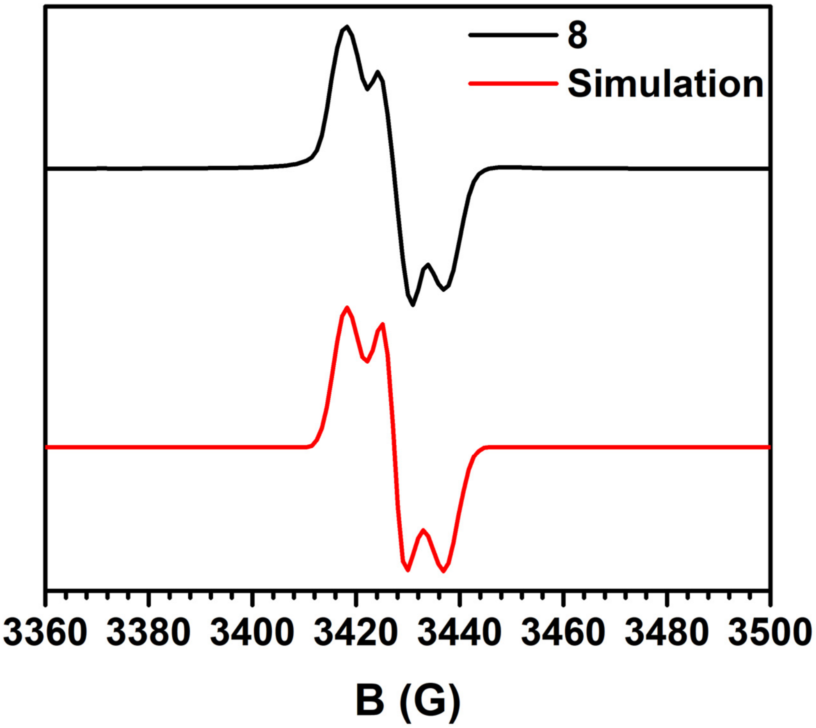

Figure S27. X-band EPR spectrum of **8** collected on a 1 mM solution in THF at 10 K. Microwave frequency: 9.63 GHz, microwave power: 1 μW, and g_{eff} = 2.013, 2.008, 2.002.

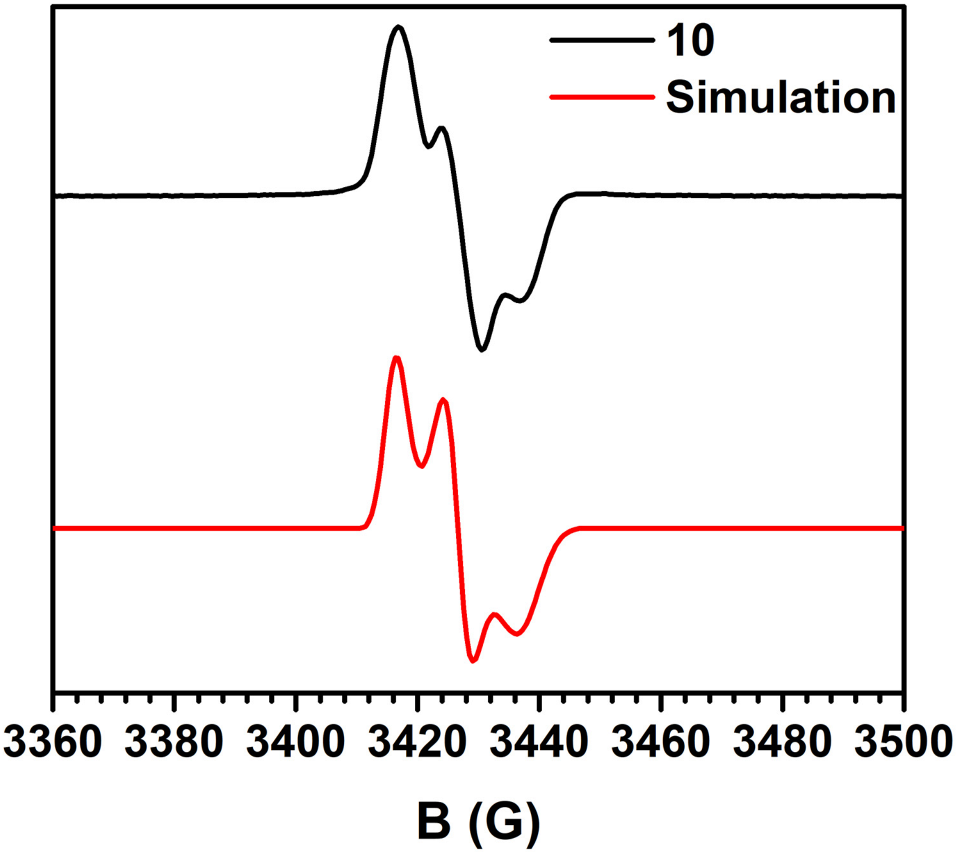

Figure S28. X-band EPR spectrum of **10** collected on a 1 mM solution in THF at 10 K. Microwave frequency: 9.63 GHz, microwave power: 0.4 μW, and g_{eff} = 2.014, 2.008, 2.001.

Infrared Spectra

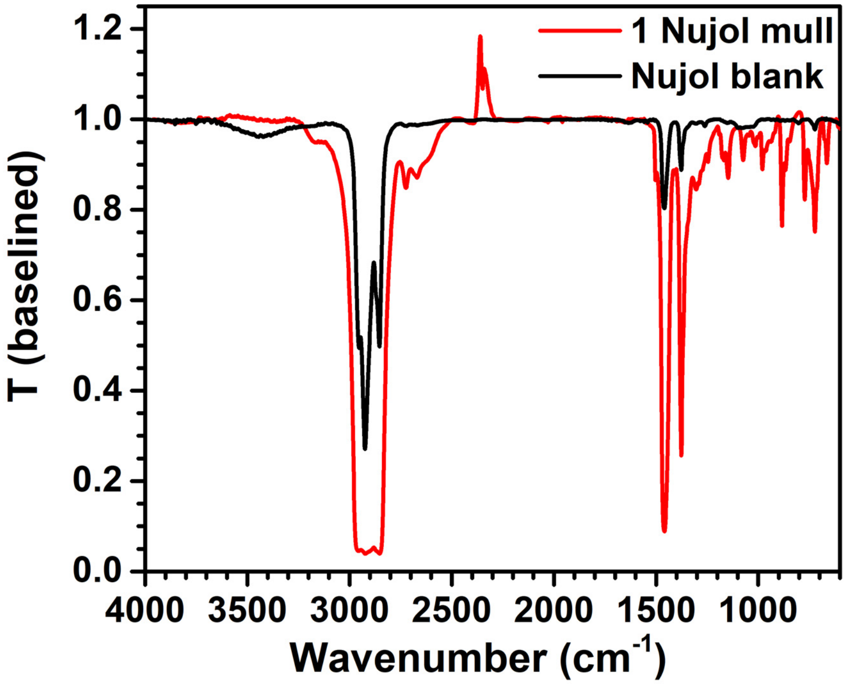

Figure S29. Infrared transmittance spectrum of **1** as a Nujol mull. Note CO_2 signals at 2350 cm^{-1}.

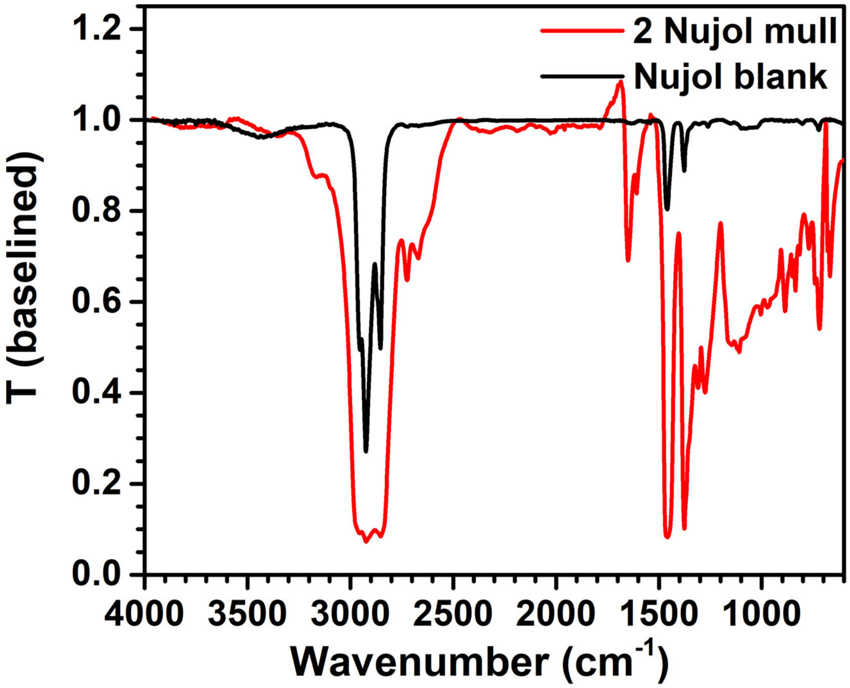

Figure S30. Infrared transmittance spectrum of **2** as a Nujol mull.

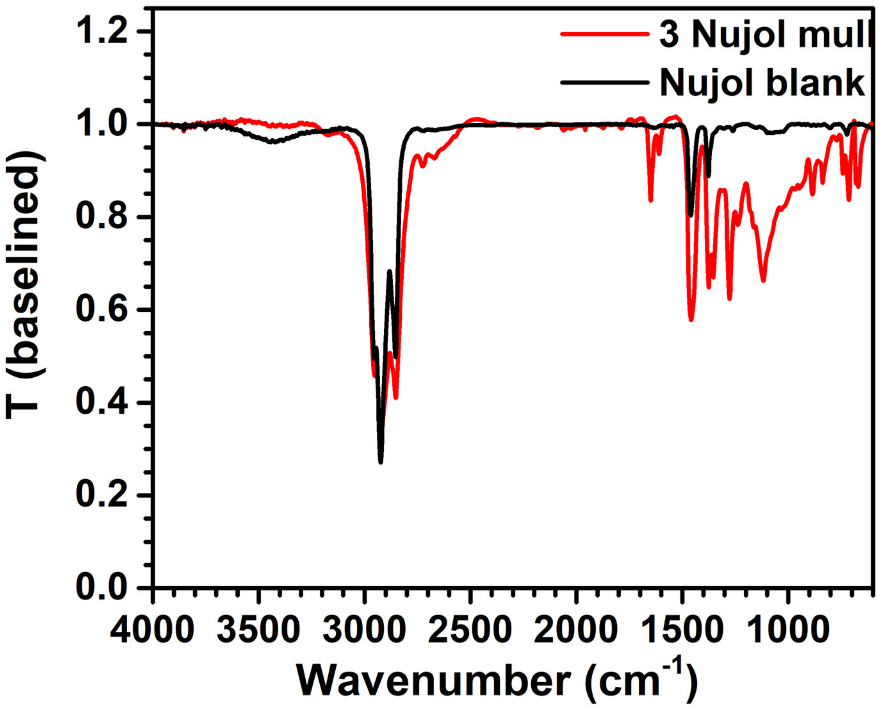

Figure S31. Infrared transmittance spectrum of **3** as a Nujol mull.

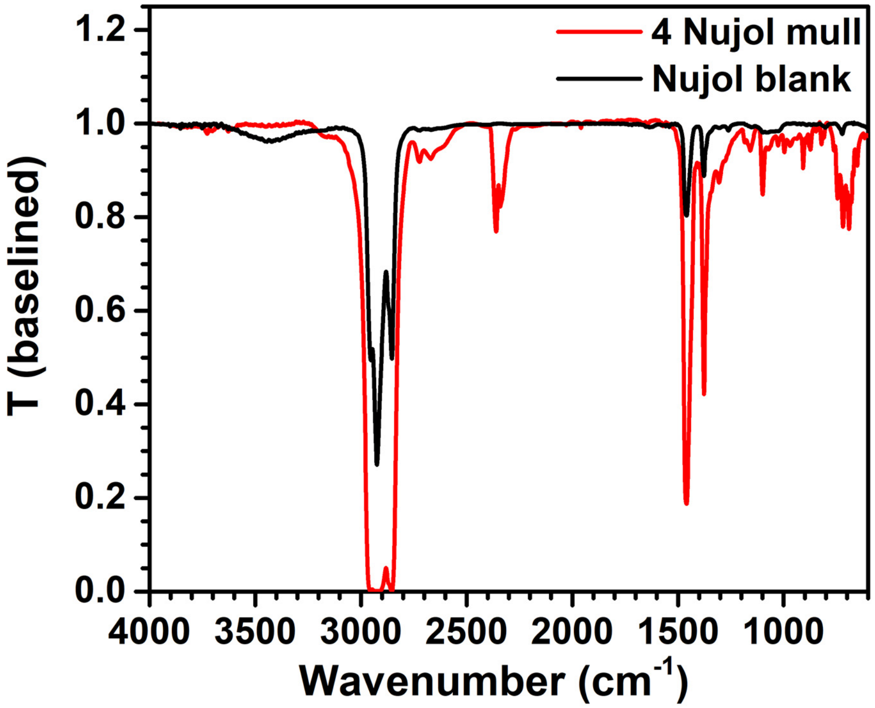

Figure S32. Infrared transmittance spectrum of 4 as a Nujol mull. Note CO_2 signals at 2350 cm^{-1}.

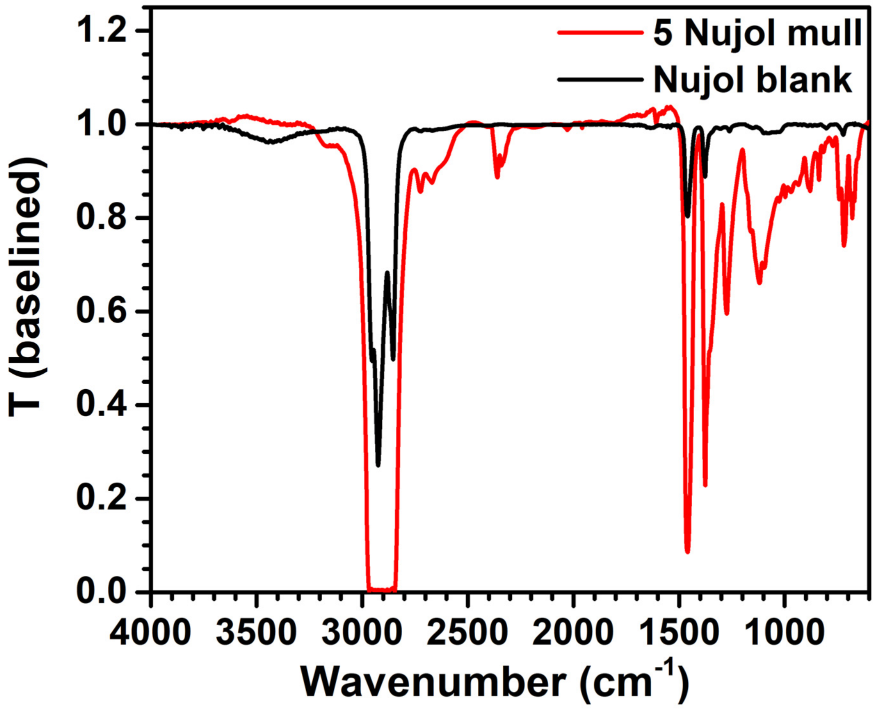

Figure S33. Infrared transmittance spectrum of **5** as a Nujol mull. Note CO_2 signals at 2350 cm^{-1}.

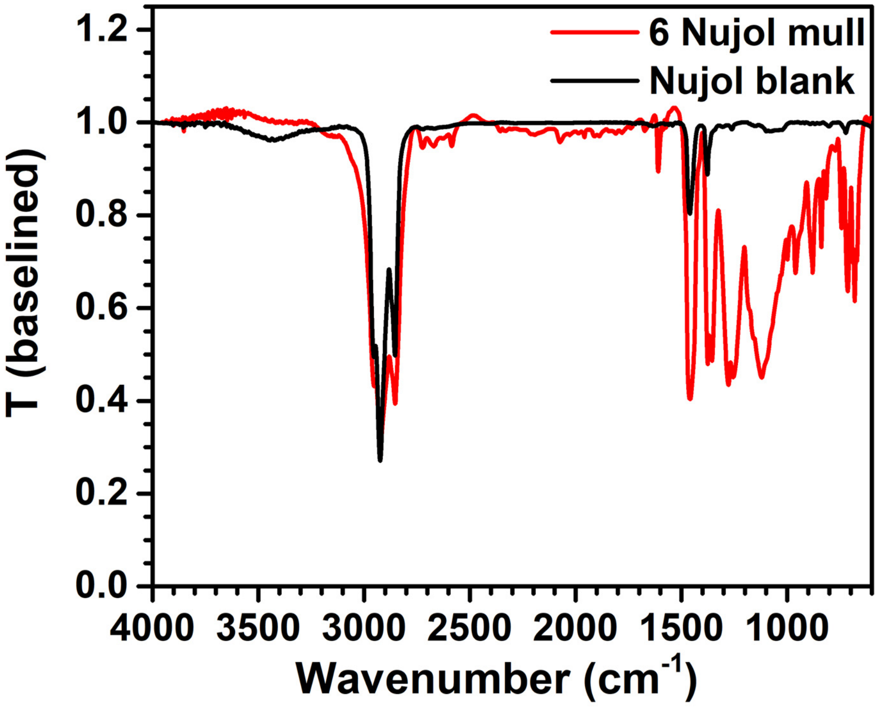

Figure S34. Infrared transmittance spectrum of **6** as a Nujol mull.

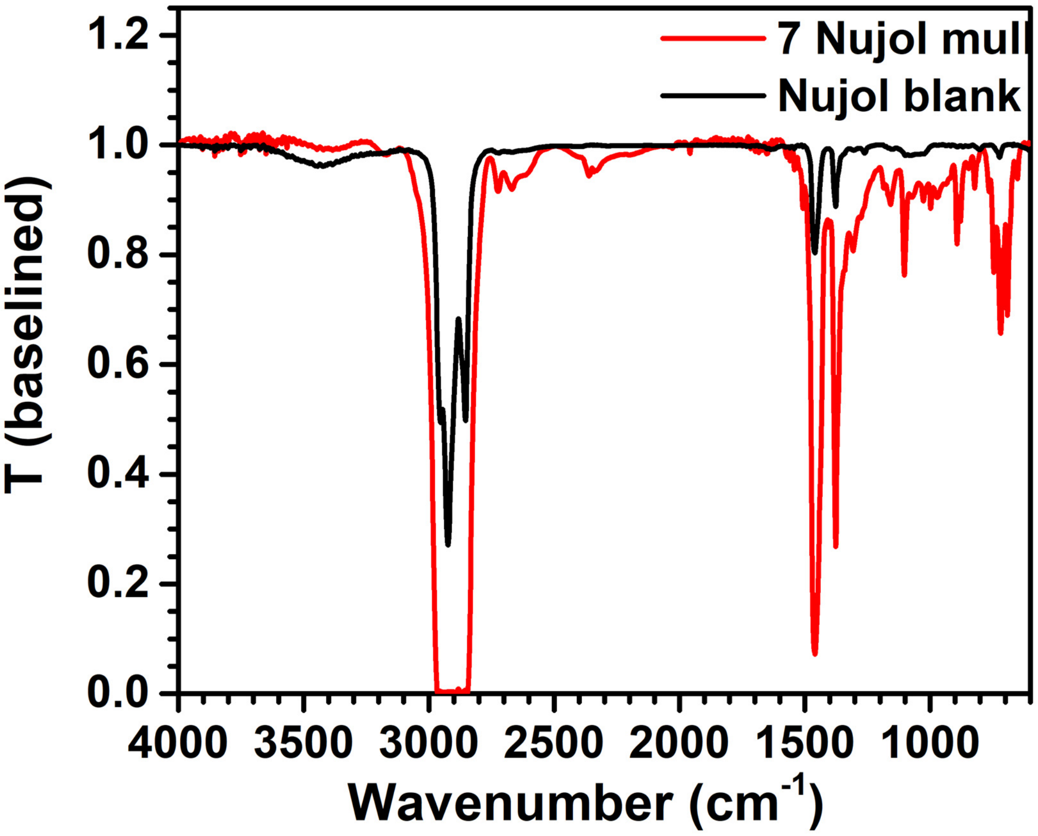

Figure S35. Infrared transmittance spectrum of **7** as a Nujol mull.

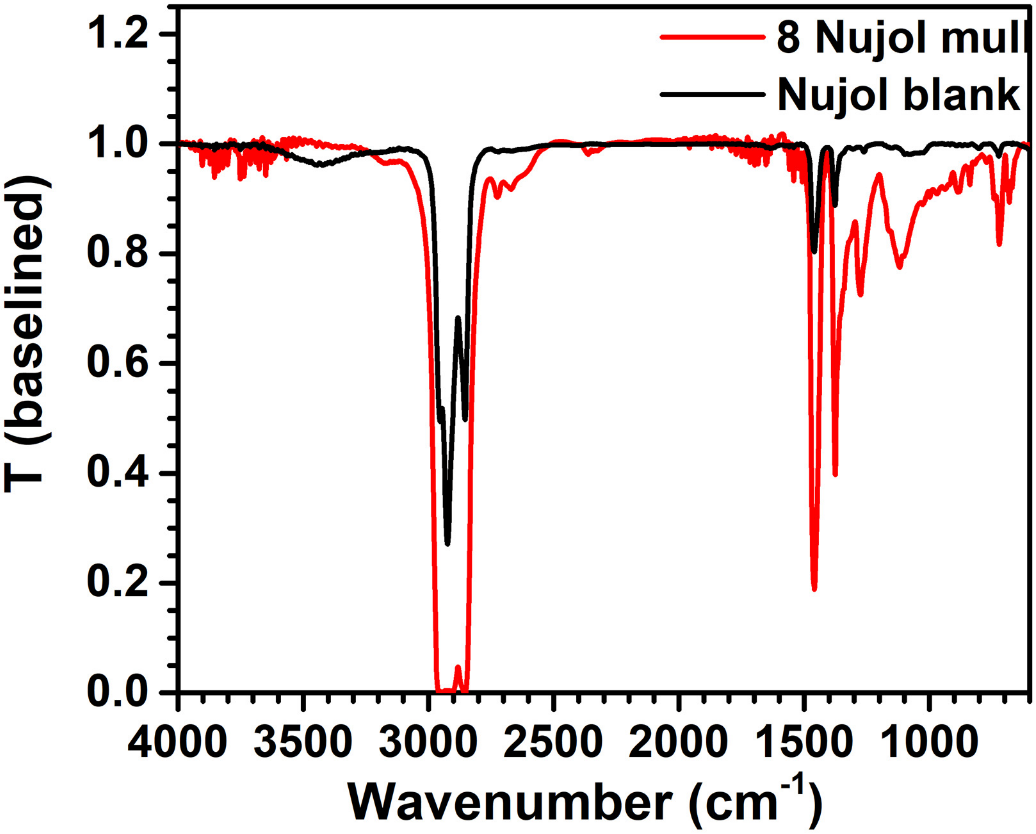

Figure S36. Infrared transmittance spectrum of **8** as a Nujol mull.

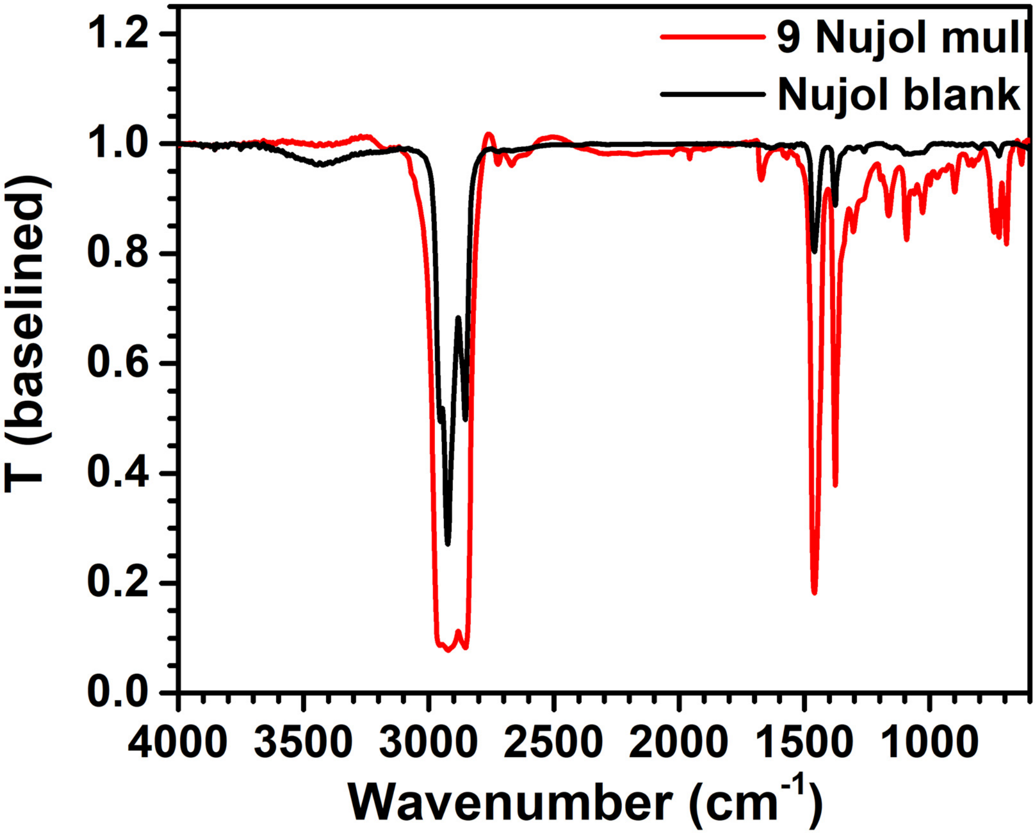

Figure S37. Infrared transmittance spectrum of **9** as a Nujol mull.

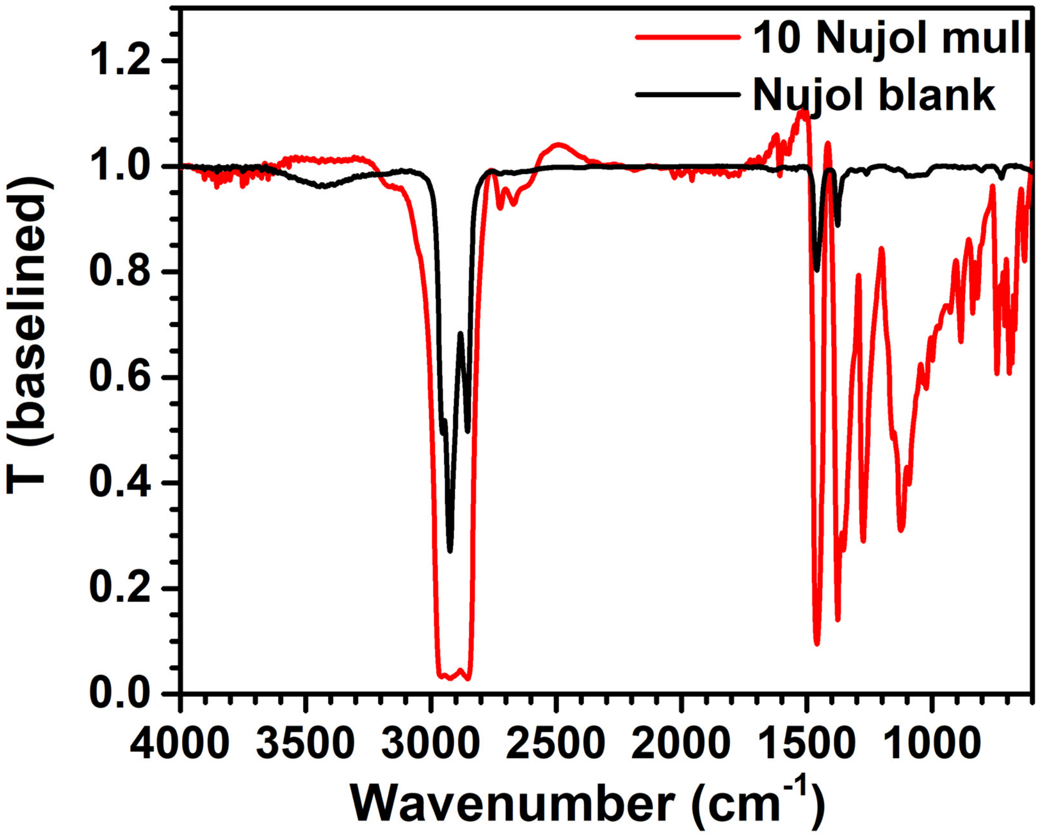

Figure S38. Infrared transmittance spectrum of **10** as a Nujol mull.

Electrochemical Measurements

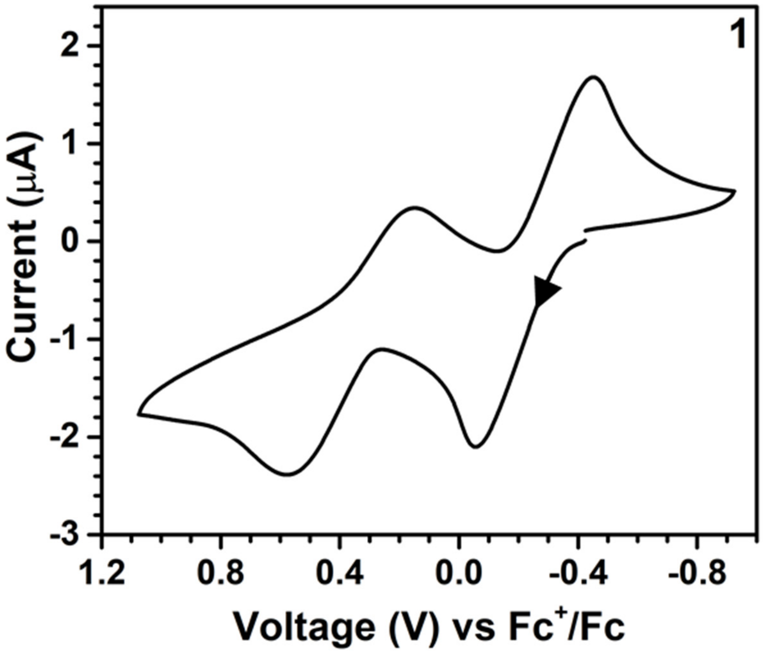

Figure S39. Cyclic voltammogram of **1** in 0.01 M [Na][BAr$^F{}_4$] in DCM and Et$_2$O (10:1). Arrow denotes scan direction. Scan rate: 0.1V/s.

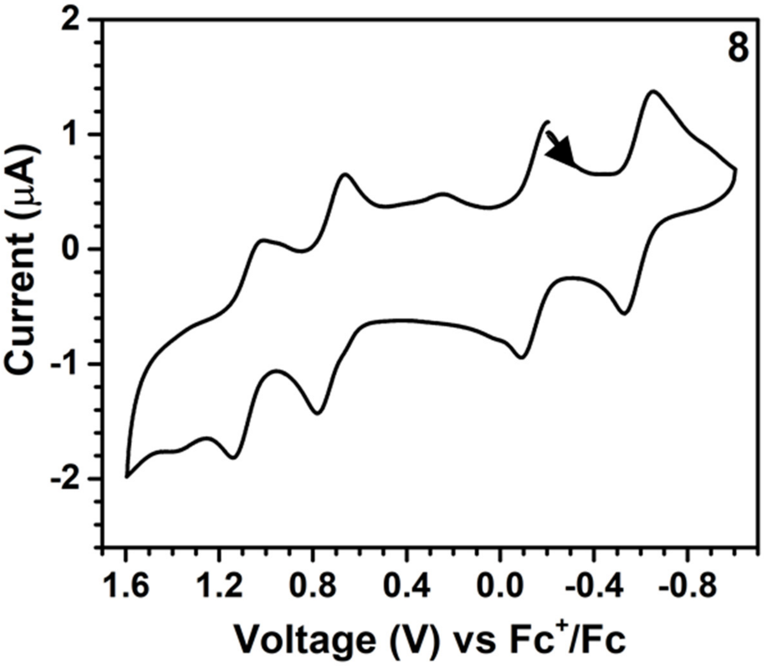

Figure S40. Cyclic voltammogram of **8** in 0.1 M [TBA][PF$_6$] in DCM. Arrow denotes scan direction. Scan rate: 0.1V/s.

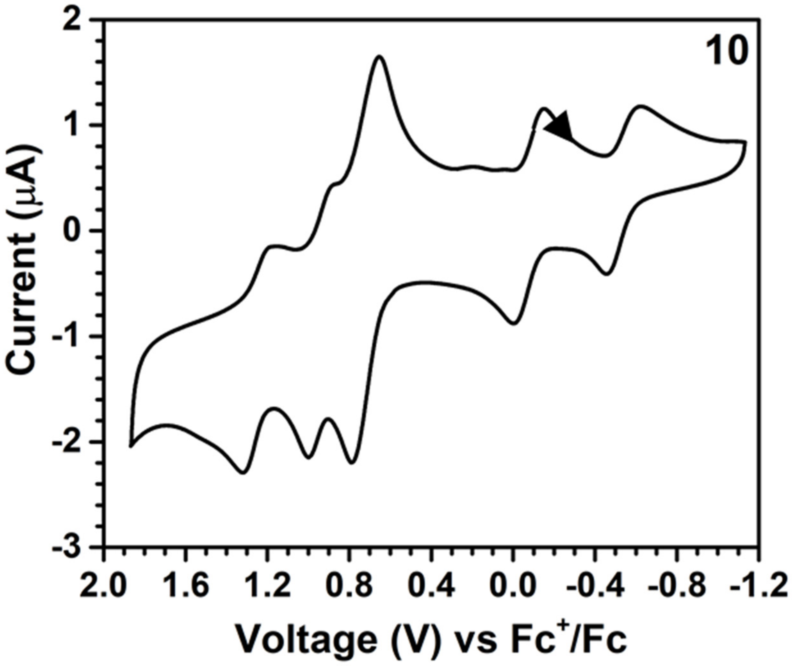

Figure S41. Cyclic voltammogram of **10** in 0.1 M [TBA][PF_6] in DCM. Arrow denotes scan direction. Scan rate: 0.1V/s.

Optical Spectroscopy

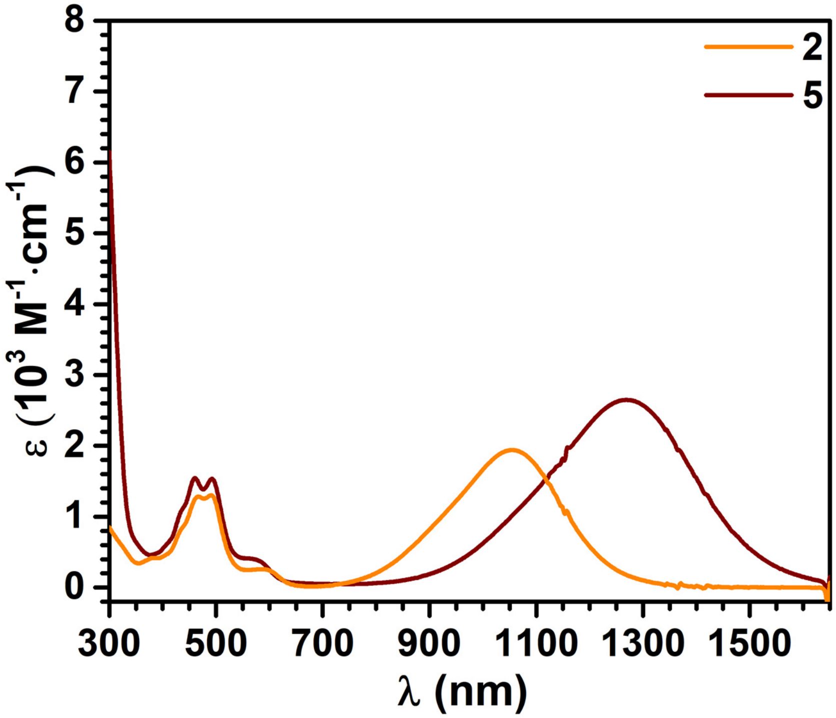

Figure S42. UV-vis-NIR absorption spectra of **2** and **5** in DCM. Concentration: 50 μM.

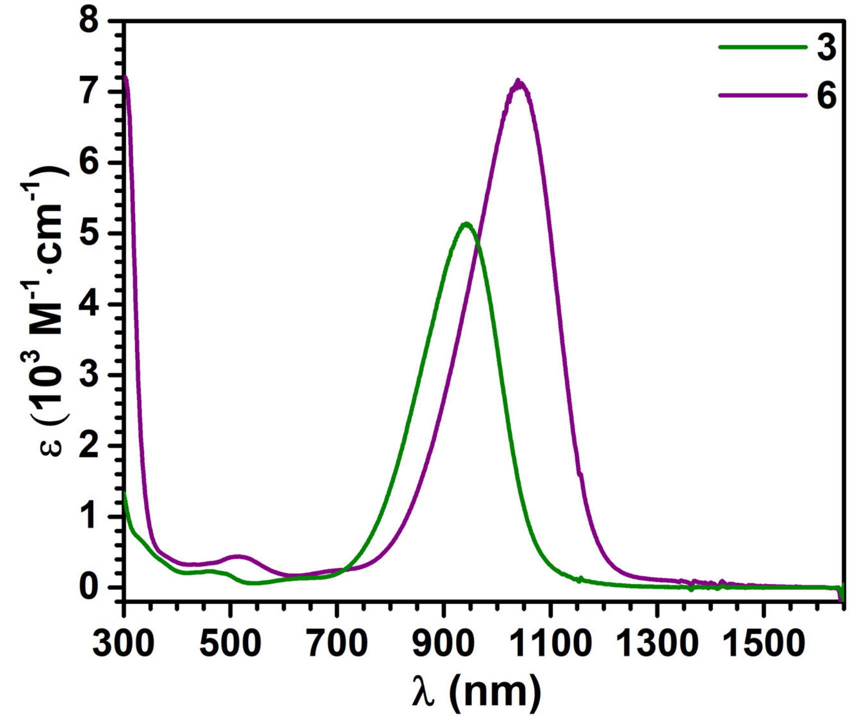

Figure S43. UV-vis-NIR absorption spectra of **3** and **6** in DCM. Concentration: 50 μM.

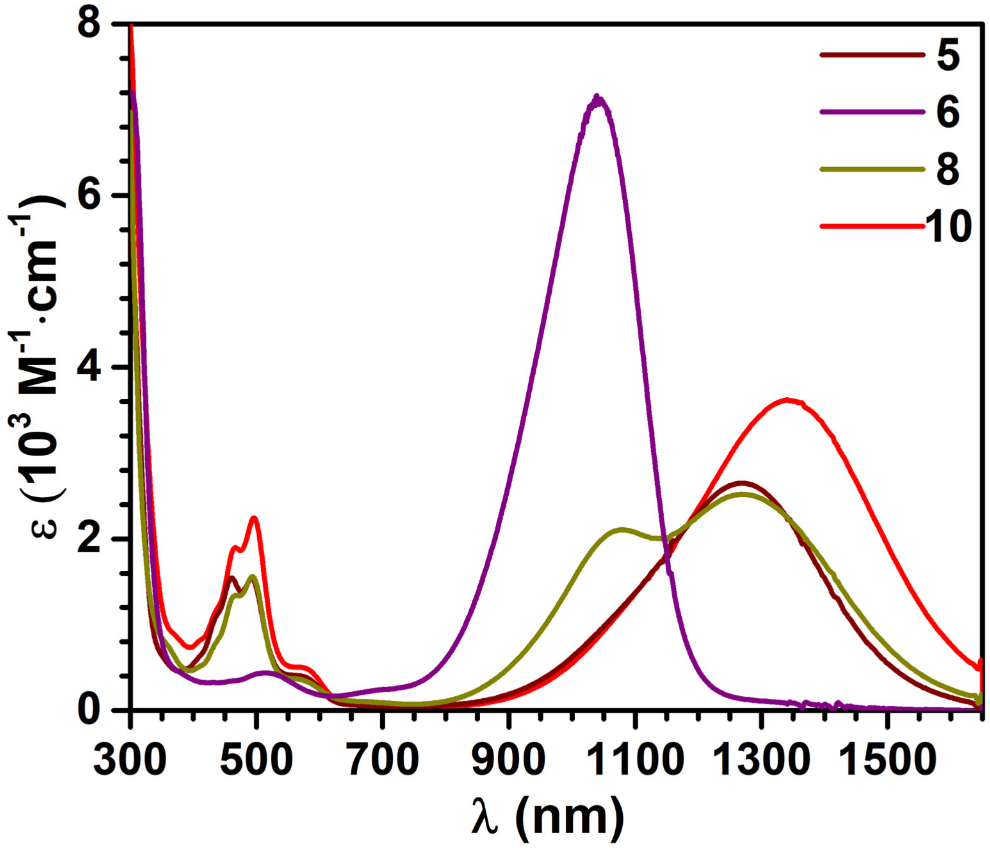

Figure S44. UV-vis-NIR absorption spectra of **5**, **6, 8** and **10** in DCM. Concentration: about 50 μM. Besides the same absorption at 1271.4 nm as **5**, **8** has a shoulder absorption peak at 1078.1 nm. Since the energy of this band is obviously lower than the same feature in dicationic **6** (1039.5 nm) and no TTF-dication UV-vis peak is observed, this shoulder peak likely arises from some other speciation due to π-dimers or oligomers.

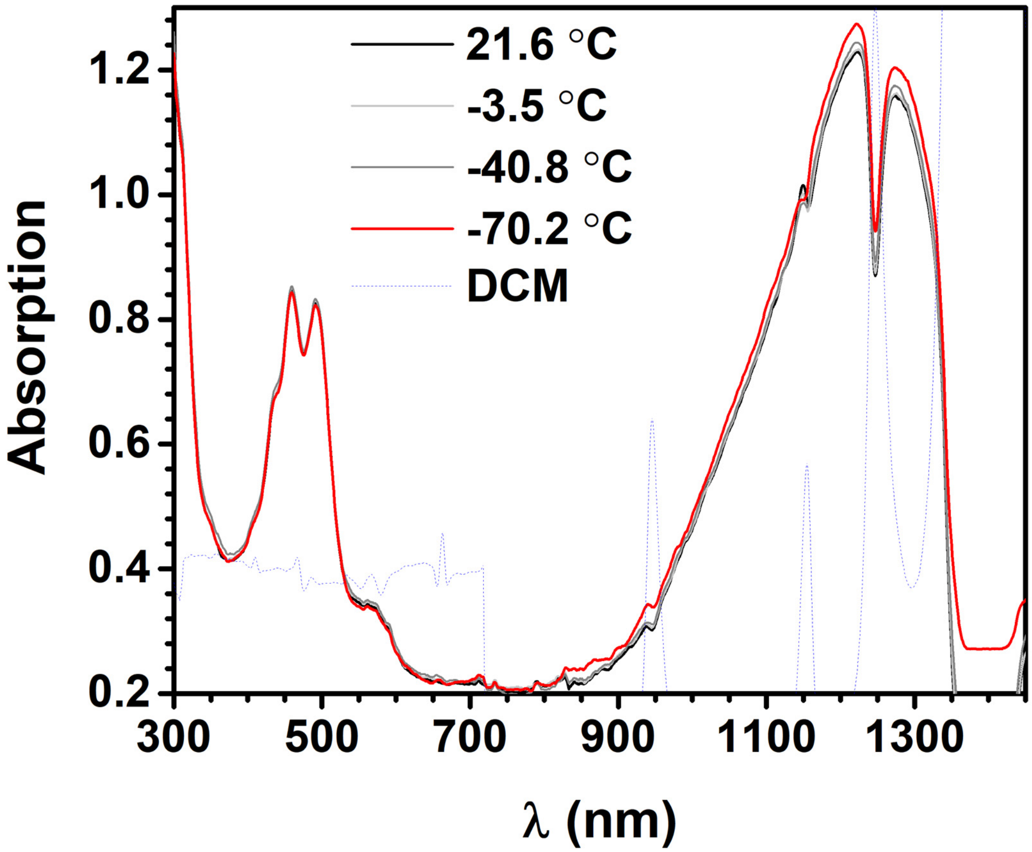

Figure S45. Variable-temperature UV-vis-NIR absorption spectra of **5** in DCM. Concentration: about 30 μM. Due to the strong background absorptions of the instrument setup and DCM, the peaks in the NIR region are somewhat convoluted. However, a clear continuous increase of NIR feature with cooling suggests the equilibrium shifts to more π-dimers when the temperature decreases.

X-ray Crystallography

1. Crystallogrphic Data

Table S1. Crystallographic data for complexes **1**, **2** and **3**.

	1•2MeCN	**2•0.5THF•0.5MeCN**	**3•2THF**
Empirical formula	$C_{26}H_{42}N_2S_8Sn_2$	$C_{57}H_{53.5}BF_{24}N_{0.5}O_{0.5}S_8Sn_2$	$C_{102}H_{92}B_2F_{48}O_4S_8Sn_2$
Formula weight	876.47	1714.17	2809.23
Temperature/K	100(2)	100(2)	100(2)
Crystal system	triclinic	monoclinic	triclinic
Space group	P-1	$P2_1/c$	P-1
a/Å	7.7711(3)	9.5804(15)	12.9111(17)
b/Å	10.3961(4)	23.505(4)	15.863(2)
c/Å	12.6341(5)	30.294(5)	16.368(2)
α/°	113.062(2)	90	88.537(3)

β/°	96.284(2)	97.920(4)	88.979(3)
γ/°	98.114(2)	90	69.195(3)
Volume/Å^3	914.39(6)	6756.8(18)	3132.5(7)
Z	1	4	1
ρ_{calc}g/cm^3	1.592	1.685	1.489
μ/mm^{-1}	1.842	1.091	0.649
F(000)	440.0	3408.0	1406.0
Crystal size/mm^3	0.32 × 0.18 × 0.07	0.24 × 0.04 × 0.04	0.29 × 0.24 × 0.04
Radiation	MoKα (λ = 0.71073)	MoKα (λ = 0.71073)	MoKα (λ = 0.71073)
2Θ range for data collection/°	5.384 to 52.974	4.402 to 44.196	4.358 to 50.398
Index ranges	$-9 \le h \le 9$, $-12 \le k \le 13$, $-15 \le l \le 15$	$-9 \le h \le 10$, $-24 \le k \le 24$, $-31 \le l \le 31$	$-15 \le h \le 15$, $-18 \le k \le 18$, $-19 \le l \le 19$
Reflections collected	26492	103447	32479
Independent reflections	3767 [R_{int} = 0.0370, R_{sigma} = 0.0253]	8304 [R_{int} = 0.1444, R_{sigma} = 0.0648]	11153 [R_{int} = 0.1152, R_{sigma} = 0.1068]
Data/restraints/parameters	3767/0/175	8304/1098/850	11153/487/815
Goodness-of-fit on F^2	1.081	1.065	1.087
Final R indexes [I>=2σ (I)]	R_1 = 0.0271, wR_2 = 0.0569	R_1 = 0.0820, wR_2 = 0.1755	R_1 = 0.0977, wR_2 = 0.2003
Final R indexes [all data]	R_1 = 0.0343, wR_2 = 0.0590	R_1 = 0.1244, wR_2 = 0.1992	R_1 = 0.1437, wR_2 = 0.2241
Largest diff. peak/hole / e Å^{-3}	1.59/-0.33	0.96/-0.94	1.40/-0.98

Table S2. Crystallographic data of complex **3**•2Fc^{BzO}.

	3•2Fc^{BzO}
Empirical formula	$C_{120}H_{88}B_2F_{48}Fe_2O_2S_8Sn_2$
Formula weight	3101.08
Temperature/K	100(2)
Crystal system	monoclinic
Space group	$P2_1/c$
a/Å	12.734(2)
b/Å	31.568(5)
c/Å	18.543(3)
α/°	90
β/°	107.358(3)
γ/°	90
Volume/Å^3	7114(2)
Z	2

ρ_{calc}g/cm^3	1.448
μ/mm^{-1}	0.562
F(000)	3092.0
Crystal size/mm^3	0.001 × 0.001 × 0.001
Radiation	synchrotron (λ = 0.41328)
2Θ range for data collection/°	1.5 to 28.76
Index ranges	-15 ≤ h ≤ 15, -37 ≤ k ≤ 37, -22 ≤ l ≤ 22
Reflections collected	150144
Independent reflections	12839 [R_{int} = 0.1297, R_{sigma} = 0.0798]
Data/restraints/parameters	12839/728/991
Goodness-of-fit on F^2	1.028
Final R indexes [I>=2σ (I)]	R_1 = 0.0678, wR_2 = 0.1719
Final R indexes [all data]	R_1 = 0.1035, wR_2 = 0.1966
Largest diff. peak/hole / e Å^{-3}	1.07/-0.74

Table S3. Crystallographic data of complexes **5** and **6**.

	5	**6**
Empirical formula	$C_{122}H_{72}B_2F_{48}Ni_2P_4S_8$	$C_{90}H_{60}BF_{24}Ni_2P_4S_8$
Formula weight	2969.19	2105.97
Temperature/K	100(2)	100(2)
Crystal system	monoclinic	triclinic
Space group	C2/c	P-1
a/Å	40.752(3)	14.1624(15)
b/Å	18.9850(12)	18.3974(19)
c/Å	17.7197(11)	20.189(2)
α/°	90	94.073(2)
β/°	107.903(2)	103.397(2)
γ/°	90	106.515(2)
Volume/Å^3	13045.5(14)	4852.8(9)
Z	4	2
ρ_{calc}g/cm^3	1.512	1.441
μ/mm^{-1}	0.582	0.169
F(000)	5960.0	2130.0
Crystal size/mm^3	0.25 × 0.23 × 0.02	0.002 × 0.002 × 0.001
Radiation	MoKα (λ = 0.71073)	synchrotron (λ = 0.41328)
2Θ range for data collection/°	4.202 to 51.594	1.686 to 31.652
Index ranges	-49 ≤ h ≤ 49, -23 ≤ k ≤ 23, -21 ≤ l ≤ 21	-18 ≤ h ≤ 18, -24 ≤ k ≤ 24, -26 ≤ l ≤ 26
Reflections collected	166738	141909
Independent reflections	12520 [R_{int} = 0.0661, R_{sigma} = 0.0320]	22441 [R_{int} = 0.0384, R_{sigma} = 0.0261]

Data/restraints/parameters	12520/381/906	22441/174/1200
Goodness-of-fit on F^2	1.013	1.047
Final R indexes [I>=2σ (I)]	$R_1 = 0.0420$, $wR_2 = 0.0906$	$R_1 = 0.0352$, $wR_2 = 0.0910$
Final R indexes [all data]	$R_1 = 0.0617$, $wR_2 = 0.0987$	$R_1 = 0.0416$, $wR_2 = 0.0963$
Largest diff. peak/hole / e Å^{-3}	0.63/-0.54	0.96/-0.58

Table S4. Crystallographic data of complexes **8** and **10**.

	8	**10**
Empirical formula	$C_{540}H_{360}B_6F_{144}P_{24}Pd_{12}S_{48}$	$C_{106}H_{68}BF_{24}Fe_2P_4Pd_2S_8$
Formula weight	13208.08	2513.27
Temperature/K	100(2)	100(2)
Crystal system	triclinic	triclinic
Space group	P-1	P-1
a/Å	29.421(4)	13.503(3)
b/Å	31.324(5)	19.054(4)
c/Å	35.123(5)	28.239(6)
α/°	92.011(3)	105.082(5)
β/°	91.984(3)	91.975(4)
γ/°	99.304(3)	90.730(5)
Volume/Å^3	31896(8)	7009(3)
Z	2	2
ρ_{calc}g/cm^3	1.375	1.191
μ/mm^{-1}	0.637	0.688
F(000)	13212.0	2514.0
Crystal size/mm^3	0.22 × 0.01 × 0.01	0.28 × 0.24 × 0.02
Radiation	MoKα (λ = 0.71073)	MoKα (λ = 0.71073)
2Θ range for data collection/°	1.162 to 42.074	4.29 to 44.728
Index ranges	$-29 \le h \le 29$, $-31 \le k \le 31$, $-35 \le l \le 35$	$-14 \le h \le 14$, $-20 \le k \le 20$, $-30 \le l \le 30$
Reflections collected	362133	59637
Independent reflections	68469 [$R_{int} = 0.1554$, $R_{sigma} = 0.1701$]	17875 [$R_{int} = 0.1086$, $R_{sigma} = 0.1360$]
Data/restraints/parameters	68469/1269/2177	17875/754/1458
Goodness-of-fit on F^2	1.204	1.070
Final R indexes [I>=2σ (I)]	$R_1 = 0.1770$, $wR_2 = 0.3523$	$R_1 = 0.0914$, $wR_2 = 0.1827$
Final R indexes [all data]	$R_1 = 0.2699$, $wR_2 = 0.3959$	$R_1 = 0.1467$, $wR_2 = 0.2038$
Largest diff. peak/hole / e Å^{-3}	3.25/-3.71	1.25/-1.04

2. Molecular planarity diagram for complexes 1, 2, 3, 5 and 6.

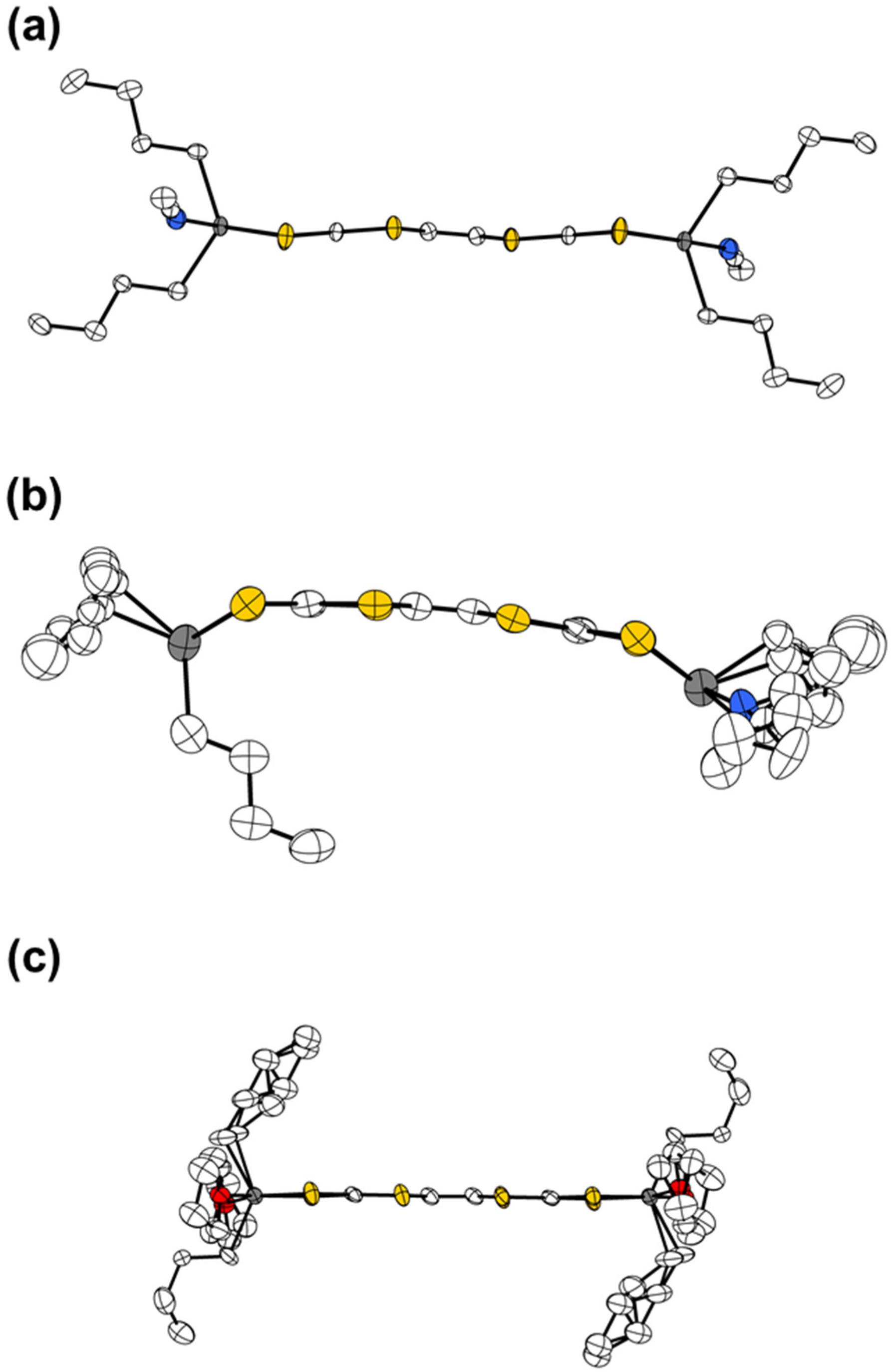

Figure S46. Molecular planarity diagram for **1**, **2** and **3**. $[\mathrm{BAr^F}_4]$ anions and H atoms are omitted for clarity. Ellipsoids are shown at 50% probability. (Sn, grey; S, yellow; O, red; N, blue; C, white.). Disorder is shown.

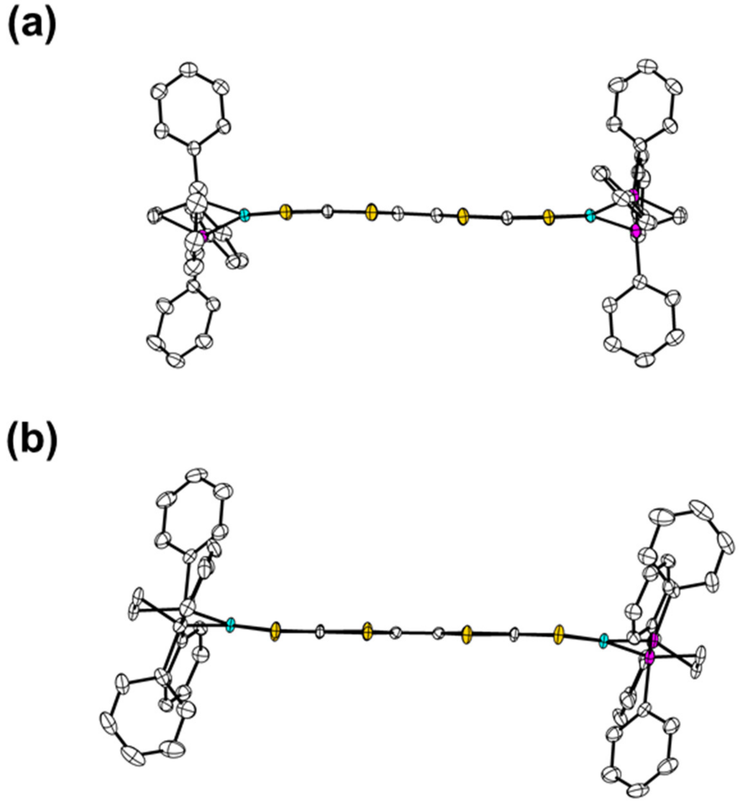

Figure S47. Molecular planarity diagram for **5** and **6**. $[\mathrm{BAr^F}_4]$ anions and H atoms are omitted for clarity. Ellipsoids are shown at 50% probability. (Ni, light blue; S, yellow; P, purple; C, white.)

3. The extended structures of 1, 2, 3, 5, and 6.

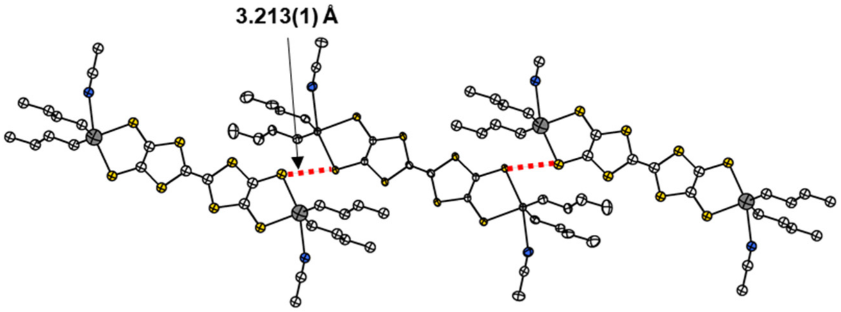

Figure S48. Supermolecular structure of **1**: 1D chain. The red dash lines represent the intermolecular S-S interactions. H atoms are omitted for clarity. Ellipsoids are shown at 50% probability. (Sn, grey; S, yellow; N, blue; C, white.)

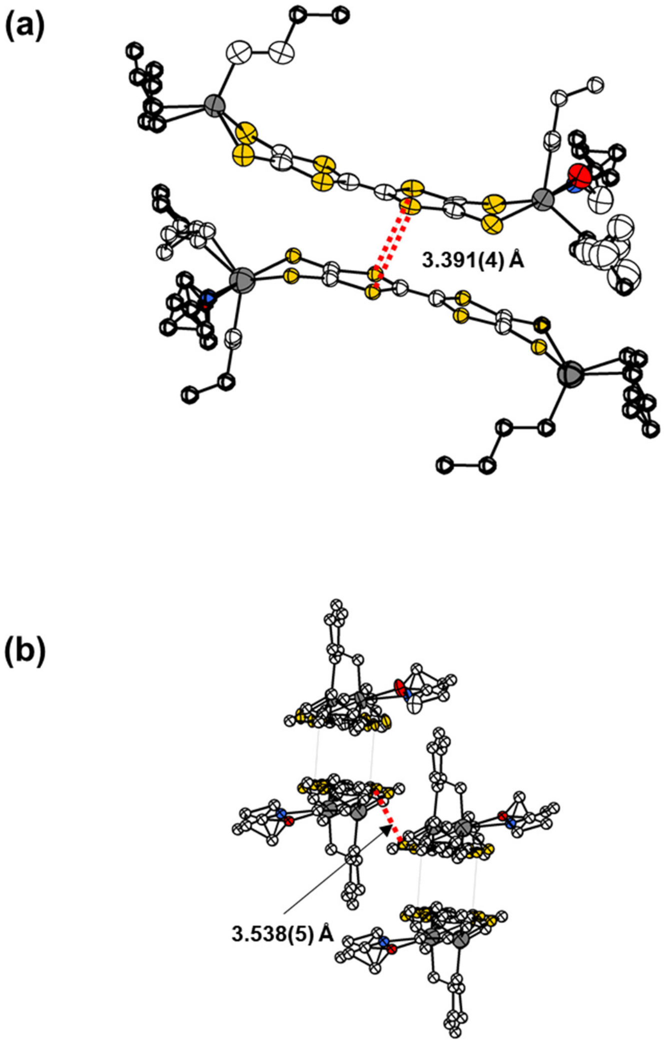

Figure S49. The extended structure of **2**: dimer unit (a) and 1D chain of dimers (b). The red dash lines represent the intermolecular S-S interactions. [$BAr^F{}_4$] anions and H atoms are omitted for clarity. Ellipsoids are shown at 50% probability. (Sn, grey; S, yellow; O, red; N, blue; C, white.). Disorder is shown.

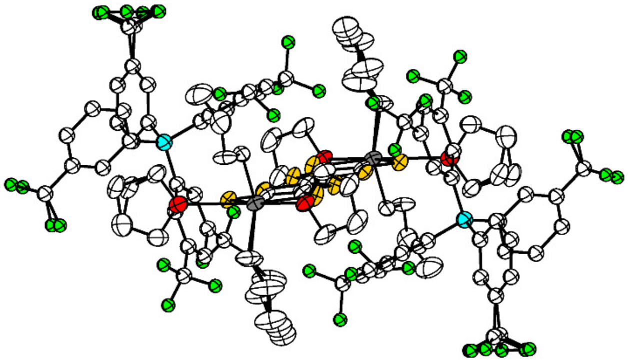

Figure S50. The molecular structure of **3**: the diactionic 3 encompassed by two bulk [BAr^F$_4$] anions. H atoms are omitted for clarity. Ellipsoids are shown at 50% probability. (Sn, grey; S, yellow; F, vivid green; B, light blue; O, red; C, white.). Disorder is shown.

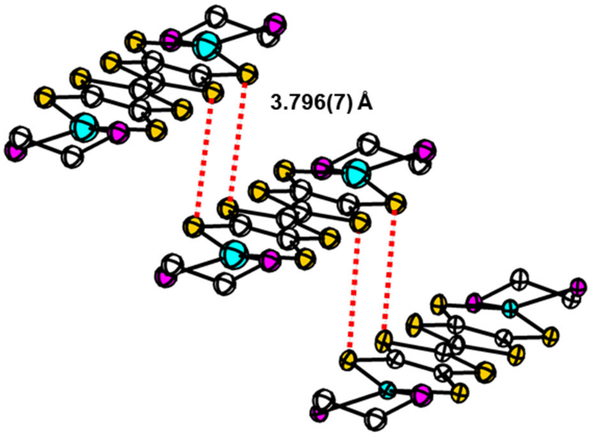

Figure S51. The extended structure of **5**:ladder-shaped 1D chain. The red dash lines represent the intermolecular S-S interactions. Phenyl groups of dppe, [BAr^F$_4$] anions and H atoms are omitted for clarity. Ellipsoids are shown at 50% probability. (Ni, light blue; S, yellow; P, purple; C, white.)

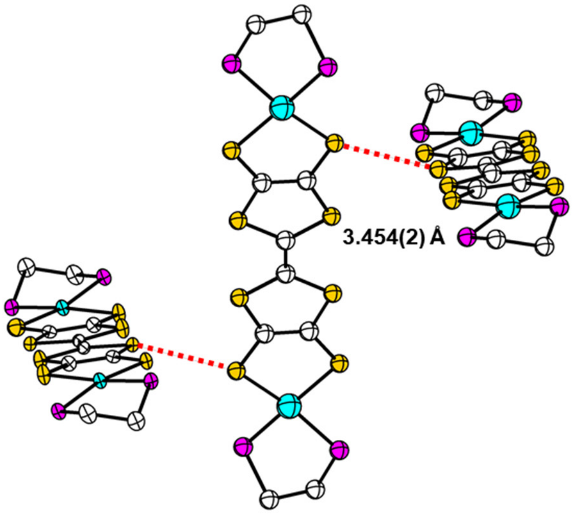

Figure S52. The extended structure of **6**: twisted 1D chain. The red dashed lines represent the intermolecular S-S interactions. Phenyl groups of dppe, [BAr$^F{}_4$] anions and H atoms are omitted for clarity. Ellipsoids are shown at 50% probability. (Ni, light blue; S, yellow; P, purple; C, white.)

3. Single-crystal X-ray Diffraction Structures of complex 3•2Fc^{BzO}, 8 and 10.

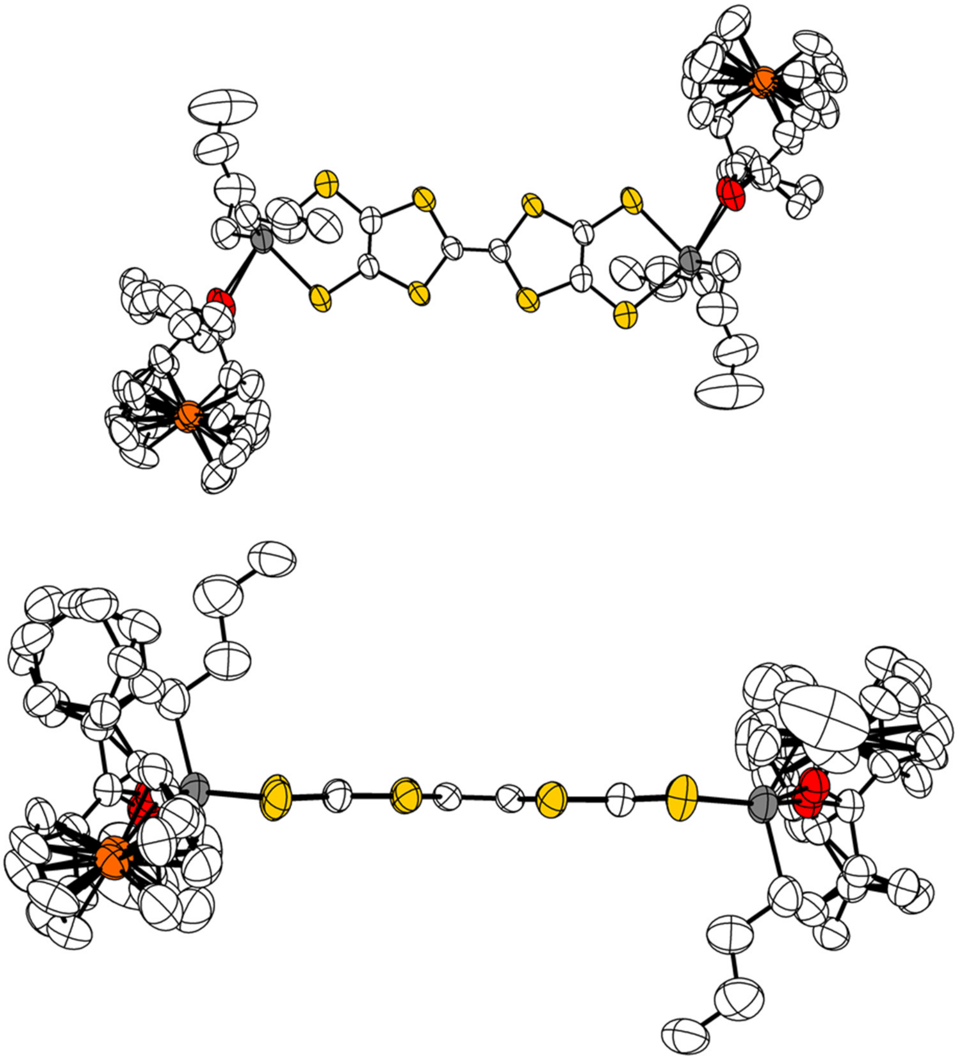

Figure S53. Single-crystal X-ray diffraction structures of complex **3**•2Fc^{BzO}. [BAr$^{F}{}_{4}$] anions and H atoms are omitted for clarity. Ellipsoids are shown at 50% probability. (Sn, grey; Fe, orange; S, yellow; O, red; C, white.). Disorder is shown.

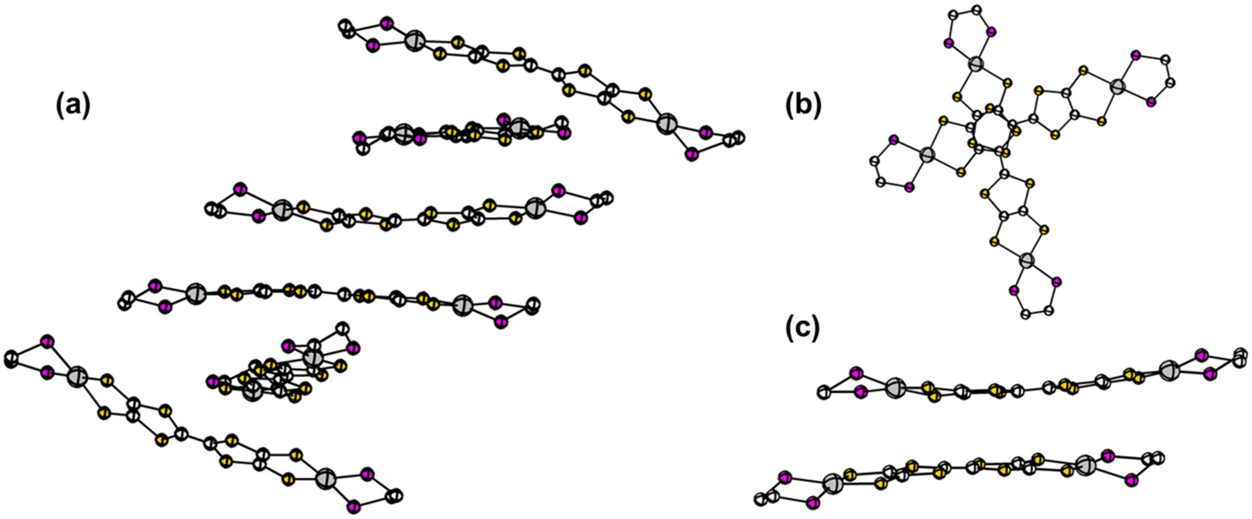

Figure S54. Single-crystal X-ray diffraction structures of complex **8**: a pentamer in 1D chain (a), a perpendicular dimer (b), and a parallel dimer (c). Phenyl groups of dppe, [BAr$^F{}_4$] anions and H atoms are omitted for clarity. Ellipsoids are shown at 50% probability. (Pd, light grey; S, yellow; P, purple; C, white.).

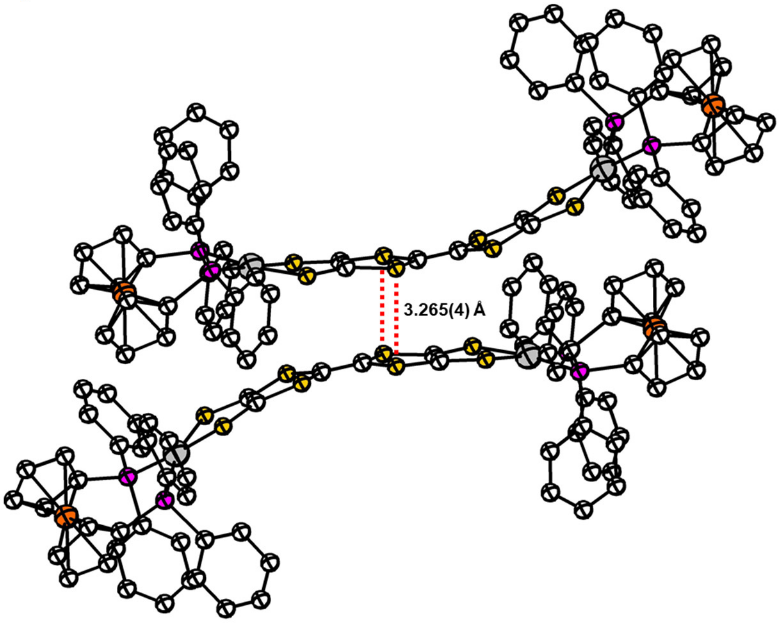

Figure S55. Single-crystal X-ray diffraction structure of complex **10** in a dimer unit. The red dashed lines represent the intermolecular S-S interactions. [BAr$^F{}_4$] anions and H atoms are omitted for clarity. Ellipsoids are shown at 50% probability. (Pd, light grey; Fe, orange; S, yellow; P, purple; C, white.).

4. Crystallographic Characterization of a Polymorph of 5.

During attempts to obtain crystals of **5**, an alternative polymorph was found with an unusual packing interaction. The crystals of this polymorph are extremely unstable and quickly decompose and lose crystallinity. Many attempts failed to provide a better-quality data set. Attempts to collect data at a synchrotron only revealed a different polymorphic form. The polymorph crystallizes in a large unit cell of over 50000 Å^3 with many co-crystallized solvent molecules. Dichloromethane is the only solvent which provides this polymorph out of many variations that have been investigated. Both amorphous solvent regions and heavy disorder of several independent [BAr$^F{}_4$] anionic units led to diffraction only up to ~ 1.2 Å. Some atoms of the [BAr$^F{}_4$] anions could not be located in the difference Fourier map due to heavy disorder. These [BAr$^F{}_4$] anions were modeled by adding bis(trifluoromethyl)benzene moieties to boron in approximate tetrahedral geometry and utilizing the visible residual electron density of benzene rings for initial placement. After that, these moieties were allowed to freely move as a whole unit with a fixed internal geometry. All atoms of the cationic TTFtt portion were located in the difference Fourier map. This has allowed for accurate assignment of the charge, general 3D packing, and connectivity of the TTFtt units from this data. The coordinates of the TTFtt packing from this solution were then used for further calculations. In the figures below, Ni is blue, P is purple, S is yellow, F is green, B is pink, H is white, and C is grey.

Table S5. Crystal data and structure refinement for the polymorph of **5**.

Empirical formula	$C_{225}H_{150}B_{2.5}F_{60}Ni_5P_{10}S_{20}$
Formula weight	5264.92
Temperature/K	100(2)
Crystal system	monoclinic
Space group	C2/c
a/Å	53.053(5)
b/Å	21.9471(19)
c/Å	51.656(5)
α/°	90
β/°	118.338(2)
γ/°	90
Volume/Å^3	52938(8)
Z	8
ρ_{calc}g/cm^3	1.321
μ/mm^{-1}	0.656
F(000)	21300.0
Radiation	MoKα (λ = 0.71073)
2Θ range for data collection/°	4.238 to 35
Index ranges	$-44 \leq h \leq 44$, $-18 \leq k \leq 18$, $-43 \leq l \leq 43$
Reflections collected	187662
Independent reflections	16783 [R_{int} = 0.1277, R_{sigma} = 0.0503]
Data/restraints/parameters	16783/1154/761
Final R indexes [I>=2σ (I)]	R_1 = 0.2814, wR_2 = 0.6230
Final R indexes [all data]	R_1 = 0.3436, wR_2 = 0.6770

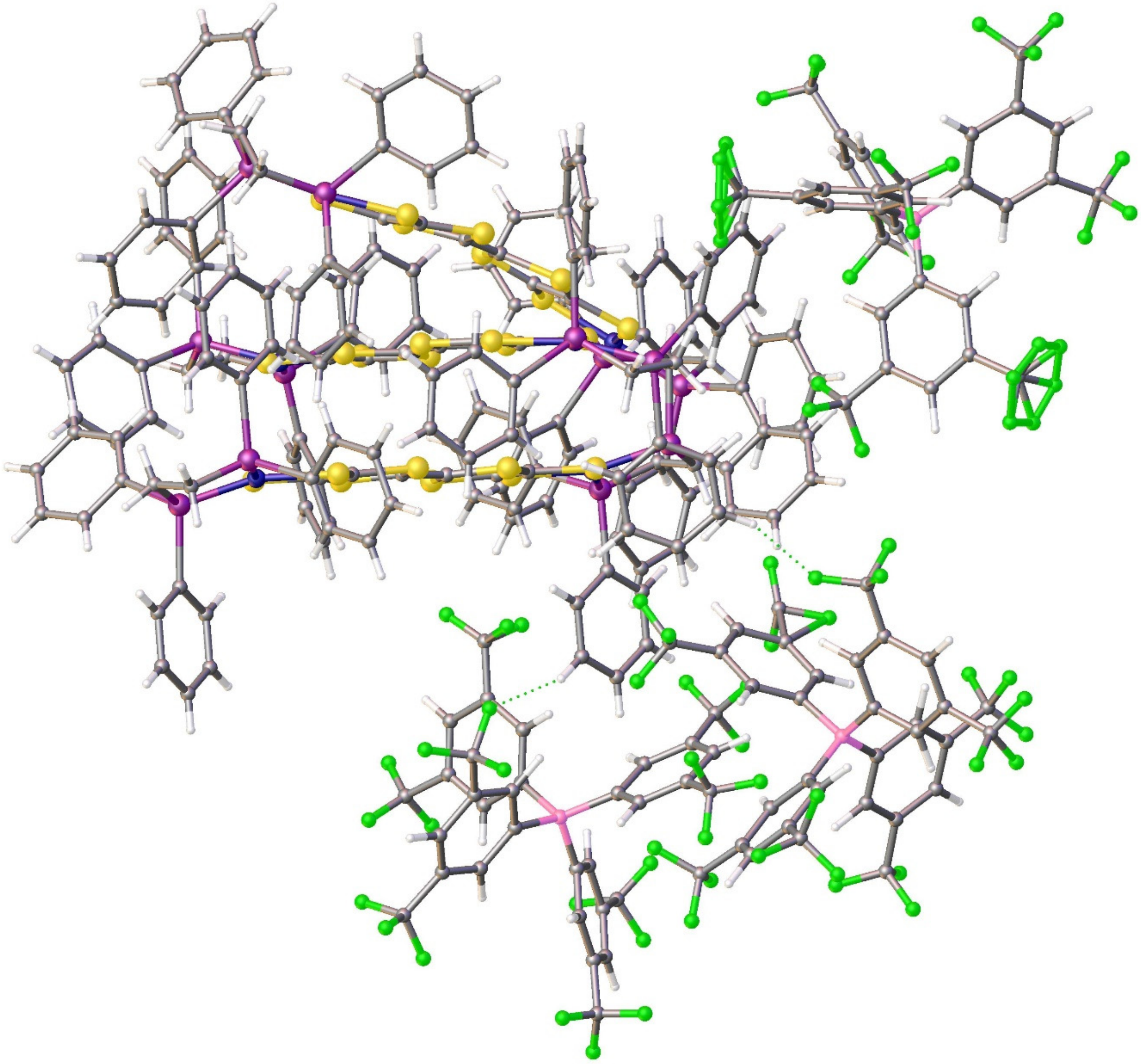

Figure S56. Symmetry-grown unit showing 3 Ni complexes along with 3 $[BAr^{F}_{4}]^{-}$ counterions.

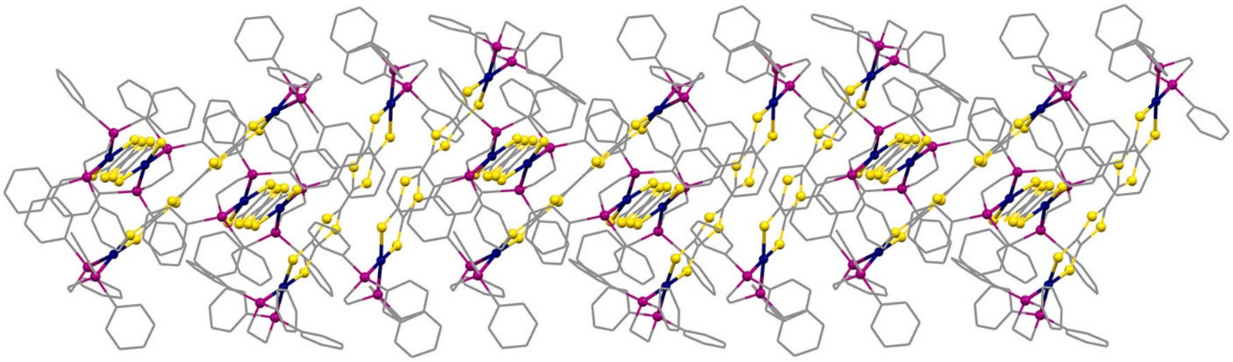

Figure S57. Part of 3D packing showing the growth of a cationic chain.

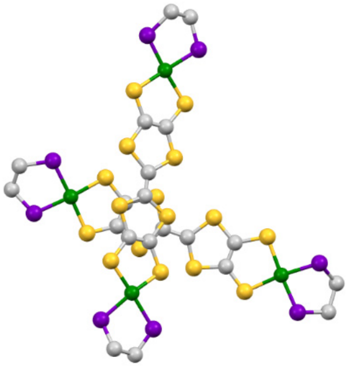

Figure S58. Diagram showing the orthogonal dimeric stacking of two TTFtt units in the polymorphic version of **5**. Note that Ni is green in this figure.

Table S6. Fractional Atomic Coordinates for the polymorph of **5** (×10^4).

Atom	***x***	***y***	***z***
Ni1	5985.5(9)	-263(2)	5716.9(10)
Ni2	3770.8(9)	2607(2)	4764.1(10)
S1	5615(2)	-315(4)	5787(2)
S2	5765(2)	275(4)	5312(2)
S3	5180(2)	855(4)	5036(2)
S4	5049(2)	331(4)	5477(2)
S5	4496(2)	1143(4)	5266(2)
S6	4556(2)	1574(4)	4767(2)
S7	4063(2)	2458(4)	4589(2)
S8	3983(2)	1955(4)	5117(2)
P1	6226(2)	-801(5)	6106(2)
P2	6371(2)	-287(5)	5693(2)
P3	3554(2)	3302(4)	4437(2)
P4	3440(2)	2739(5)	4877(2)
C3	6469(11)	652(16)	6744(11)
C4	6735(10)	486(19)	6972(8)
C5	6848(8)	-90(20)	6972(8)
C6	6695(11)	-491(16)	6743(10)
C1	6430(11)	-320(20)	6515(7)
C2	6317(8)	250(20)	6515(8)
C7	5987(9)	-1440(20)	6211(12)
C8	5921(10)	-1347(16)	6438(10)
C9	5737(10)	-1740(20)	6476(9)
C10	5619(8)	-2240(20)	6287(12)
C11	5685(9)	-2332(17)	6060(10)
C12	5869(10)	-1940(20)	6022(9)

C13	6473(7)	-1283(17)	6056(5)
C14	6493(7)	-1099(18)	5787(5)
C15	6409(12)	-30(20)	5316(8)
C20	6601(9)	380(20)	5302(7)
C19	6581(10)	531(18)	5031(10)
C18	6369(11)	270(20)	4775(7)
C17	6177(9)	-140(20)	4789(8)
C16	6197(10)	-295(19)	5059(12)
C22	6611(7)	820(30)	6072(9)
C23	6809(11)	1210(16)	6282(11)
C24	7091(9)	1020(20)	6453(8)
C25	7175(7)	450(20)	6413(9)
C26	6977(11)	56(16)	6203(10)
C21	6695(9)	240(20)	6033(8)
C27	3741(9)	4174(12)	4452(12)
C32	3780(9)	4561(17)	4261(8)
C31	3945(10)	5084(15)	4368(11)
C30	4071(8)	5220(15)	4666(12)
C29	4032(10)	4830(20)	4858(8)
C28	3867(11)	4310(20)	4750(11)
C33	3422(12)	3010(20)	3996(5)
C38	3644(9)	3050(20)	3925(9)
C37	3596(10)	2890(20)	3645(11)
C36	3327(12)	2690(20)	3436(6)
C35	3106(9)	2650(20)	3506(7)
C34	3153(10)	2810(20)	3786(9)
C39	3228(4)	3579(13)	4461(6)
C40	3110(5)	3050(13)	4552(6)
C41	3530(12)	3362(18)	5228(8)
C46	3326(9)	3760(20)	5225(8)
C45	3398(10)	4171(18)	5455(11)
C44	3675(12)	4179(17)	5689(8)
C43	3880(8)	3780(20)	5692(8)
C42	3807(11)	3371(18)	5462(11)
C48	3219(10)	1490(20)	4812(9)
C47	3293(10)	1962(16)	5015(12)
C52	3275(9)	1880(16)	5272(10)
C51	3182(10)	1330(20)	5327(9)
C50	3108(10)	854(13)	5124(12)
C49	3126(10)	936(19)	4867(10)
C53	4265(7)	1722(16)	5054(8)
C54	4303(7)	1895(17)	4845(8)

C55	4702(7)	1111(16)	5100(8)
C56	4939(8)	784(16)	5184(8)
C57	5364(7)	169(16)	5509(8)
C58	5449(7)	396(16)	5322(8)
Ni3	4856.3(11)	2310(3)	6199.1(13)
Ni4	4651.3(14)	4069(3)	3877.1(16)
S9	5031(2)	1992(5)	5929(2)
S10	4623(3)	3042(7)	5917(3)
S11	4565(2)	3432(6)	5321(3)
S12	4982(2)	2522(5)	5368(2)
S13	4898(3)	2943(5)	4738(3)
S14	4876(3)	3309(6)	4162(3)
S15	4433(2)	4374(5)	4118(3)
S16	4489(2)	3884(5)	4693(2)
P5	4609(3)	2301(7)	6435(3)
P6	5125.6(12)	1629(3)	6556.3(10)
P7	4428.9(13)	4747(3)	3538.6(11)
P8	4930.4(14)	3962(3)	3695.1(12)
C63	4094(8)	3900(20)	6474(10)
C64	4154(9)	3301(16)	6434(9)
C59	4424(11)	3148(14)	6473(10)
C60	4634(8)	3590(30)	6552(10)
C61	4574(10)	4190(20)	6592(9)
C62	4304(12)	4345(12)	6553(10)
C65	4304(8)	1566(16)	6279(11)
C66	4171(11)	1610(18)	5975(12)
C67	3925(10)	1270(20)	5804(8)
C68	3812(7)	890(20)	5938(10)
C69	3945(9)	849(18)	6243(11)
C70	4191(9)	1185(19)	6414(8)
C71	4854(9)	2037(14)	6805(5)
C72	4992(5)	1442(15)	6813(5)
C78	5498(3)	510(6)	6516.2(14)
C73	5233(3)	765(5)	6444.6(15)
C74	4983(3)	441(6)	6273(2)
C75	4998(3)	-138(6)	6172(2)
C76	5263(3)	-393(6)	6244(2)
C77	5513(3)	-70(6)	6415.8(18)
C81	5946.4(13)	1875(4)	7213.4(13)
C80	5670.5(12)	1651(3)	7044.7(10)
C79	5487.9(12)	1924(3)	6777.6(10)
C84	5581.1(15)	2421(4)	6679.3(16)

C83	5856.9(17)	2646(4)	6848(2)
C82	6039.5(14)	2372(5)	7115.0(18)
C85	4715(10)	2940(20)	5637(10)
C86	4897(9)	2530(20)	5655(9)
C87	4735(9)	3150(20)	5165(10)
C88	4728(9)	3205(19)	4932(10)
C89	4575(9)	3830(20)	4417(9)
C90	4772(10)	3420(20)	4449(10)
C92	4086(4)	5696(5)	3650.0(14)
C91	4367(4)	5591(5)	3710.1(16)
C96	4579(4)	6017(6)	3869(2)
C95	4509(4)	6548(6)	3968(2)
C94	4228(4)	6653(6)	3908(2)
C93	4017(4)	6227(6)	3748.8(19)
C97	4053.2(14)	4235(5)	3257.0(18)
C98	3911(3)	3702(6)	3254(5)
C99	3657(3)	3547(10)	3005(6)
C100	3546(2)	3926(18)	2760(3)
C101	3689(2)	4459(18)	2764(3)
C102	3942(2)	4614(10)	3012(4)
C103	4659(5)	4978(15)	3384(5)
C104	4826(8)	4443(12)	3372(5)
C110	4727.3(16)	2732(6)	3342.9(15)
C105	4944.7(16)	3027(6)	3583.2(14)
C106	5192.7(17)	2713(7)	3770.2(18)
C107	5223(2)	2104(7)	3717(2)
C108	5006(2)	1809(6)	3477(2)
C109	4758(2)	2123(6)	3289.7(19)
C112	5552(4)	4288(4)	3921(2)
C111	5326(4)	4416(4)	3977(2)
C116	5365(4)	4813(6)	4202(3)
C115	5631(4)	5083(6)	4372(3)
C114	5857(4)	4955(6)	4316(3)
C113	5817(4)	4557(5)	4090(2)
F25	6429(7)	4884(13)	4959(6)
F26	6676(8)	4878(13)	5406(5)
F27	6364(5)	4229(15)	5180(7)
F28	6916(6)	2183(10)	5279(7)
F29	7293(6)	2663(17)	5575(5)
F30	7256(5)	2515(16)	5208(6)
C181	7470(2)	6535(4)	5226(2)
F37	7794(4)	5774(7)	5930.8(18)

F38	7379(4)	6204(7)	5784(3)
F39	7741(4)	6746(6)	5831(3)
F40	7568(4)	7079(5)	4702(3)
F41	7231(3)	7420(4)	4790(3)
F42	7131(4)	6756(5)	4440(3)
C178	7434.9(15)	5324(4)	5041.9(16)
C179	7370.1(19)	5797(4)	4839.5(18)
C180	7387(2)	6401(4)	4932(2)
C182	7535(2)	6057(5)	5427(2)
C183	7518(2)	5453(4)	5336.4(16)
C184	7328(3)	6913(4)	4717(3)
C185	7614(3)	6196(6)	5743(2)
C190	7114(4)	3289(6)	5204(4)
C191	7278(5)	3639(9)	5114(7)
C186	7214(7)	4252(10)	5048(8)
C187	6987(6)	4515(7)	5070(7)
C188	6824(4)	4165(10)	5160(6)
C189	6887(4)	3552(10)	5226(5)
C192	6586(3)	4503(10)	5176(4)
C193	7073(4)	2674(7)	5305(4)
C197	7003(2)	4786(5)	3961.4(18)
F43	7468(4)	5741(8)	3970(3)
F44	7745(3)	4947(9)	4139(3)
F45	7363(3)	4909(8)	3710(3)
F46	6406(2)	4763(8)	3656(2)
F47	6491(3)	3851(8)	3844(2)
F48	6375.8(16)	4576(9)	4056(3)
C194	7262.6(16)	4677(3)	4573.8(18)
C195	6971.1(16)	4554(4)	4404.1(19)
C196	6841.2(19)	4609(5)	4098.4(18)
C198	7294(2)	4908(5)	4133(2)
C199	7425.1(18)	4855(4)	4440(2)
C200	6529(2)	4453(7)	3914(2)
C201	7467(3)	5123(7)	3988(3)
C205	8214.0(19)	3514(5)	5350(2)
F31	7844(3)	2746(6)	4650(3)
F32	7902(3)	2258(4)	5041(4)
F33	8274(3)	2594(6)	5011(4)
F34	8611(2)	3806(8)	5927(2)
F35	8615.5(18)	4648(7)	5706(3)
F36	8361(3)	4589(8)	5934(2)
C202	7711.1(16)	4207(4)	5087.3(15)

C203	7731.4(19)	3670(4)	4954.3(18)
C204	7983(2)	3325(4)	5085(2)
C206	8191.0(18)	4051(5)	5482.6(19)
C207	7940.4(17)	4399(4)	5352.1(17)
C208	8001(3)	2734(5)	4947(3)
C209	8444(2)	4271(7)	5763(2)
B2	7415.0(17)	4612(4)	4933.8(18)
F7	8717(6)	5200(17)	7364(5)
F8	8873(5)	5234(17)	7833(5)
F9	8473(6)	5696(11)	7539(6)
F10	8870(4)	3064(17)	7888(6)
F11	8557(7)	2496(10)	7622(6)
F12	8579(6)	2932(17)	8028(5)
F13	7766(4)	3259(15)	8042(8)
F14	7430(6)	3952(10)	7973(7)
F15	7394(7)	2935(10)	7985(7)
F16	6706(5)	2352(15)	7033(6)
F17	6754(8)	2754(15)	6642(4)
F18	6971(7)	2047(10)	6889(7)
F19	7659(5)	1800(14)	6612(5)
F20	8077(4)	2035(17)	6657(6)
F21	7700(6)	2067(17)	6227(4)
F22	7396(3)	4408(13)	5876(6)
F23	7799(5)	4801(8)	6131(7)
F24	7757(4)	4011(12)	5885(4)
C149	7140(3)	5635(6)	6961(3)
F1	6665(4)	4751(9)	6326(4)
F2	6826(5)	5612(10)	6252(3)
F3	6583(3)	5596(10)	6495(4)
F4	7373(4)	6574(7)	7370(4)
F5	7391(4)	5833(11)	7658(3)
F6	7772(4)	6078(10)	7625(4)
C146	7496(5)	4642(9)	7024(5)
C147	7236(4)	4709(8)	6767(4)
C148	7058(3)	5204(6)	6737(3)
C150	7400(3)	5564(7)	7218(3)
C151	7579(4)	5070(9)	7250(4)
C152	7485(4)	6014(8)	7467(3)
C153	6783(4)	5290(8)	6454(3)
C157	7200(3)	3003(10)	7399(3)
C158	7433(4)	3354(11)	7587(3)
C159	7594(5)	3660(13)	7479(5)

C154	7520(6)	3614(16)	7183(5)
C155	7286(6)	3262(14)	6995(3)
C156	7126(4)	2956(10)	7103(3)
C160	6867(4)	2576(8)	6921(4)
C161	7491(4)	3412(9)	7900(3)
C166	8456(4)	4656(6)	7511(6)
C167	8166(4)	4619(10)	7312(6)
C162	8022(4)	4069(13)	7271(7)
C163	8168(6)	3557(9)	7429(7)
C164	8458(6)	3594(7)	7628(6)
C165	8602(3)	4144(10)	7669(5)
C168	8639(4)	5215(7)	7573(4)
C169	8588(4)	3002(7)	7776(4)
C172	7696(5)	3847(7)	6303(3)
C171	7687(7)	4077(7)	6548(5)
C170	7712(9)	3685(12)	6771(5)
C175	7746(8)	3063(11)	6747(5)
C174	7756(6)	2833(6)	6501(5)
C173	7731(6)	3225(8)	6279(4)
C176	7798(4)	2156(5)	6514(4)
C177	7666(3)	4266(6)	6060(3)
B1	7678(3)	4027(6)	7036(3)
Ni5	5834.4(12)	2938(2)	5154.7(14)
S17	5649(3)	3245(6)	5420(3)
S18	5623(3)	3623(6)	4810(3)
S19	5197(3)	4618(6)	4750(3)
S20	5250(3)	4325(6)	5323(3)
P9	6131.7(16)	2370(5)	5504.6(12)
P10	5947.0(14)	2373(5)	4891(2)
C120	5128(9)	1020(20)	4344(9)
C119	5406(11)	799(15)	4502(10)
C118	5634(7)	1200(30)	4639(9)
C117	5583(8)	1830(20)	4618(9)
C122	5305(11)	2047(15)	4460(10)
C121	5078(6)	1640(20)	4323(9)
C124	6007.0(15)	2365(7)	4365(4)
C125	6063.2(19)	2513(9)	4136(4)
C126	6177(3)	3080(11)	4130(4)
C127	6234(5)	3499(9)	4353(5)
C128	6178(5)	3351(8)	4582(5)
C123	6064(2)	2784(7)	4588(4)
C129	6264(9)	1870(20)	5143(9)

C130	6239(9)	1716(18)	5368(8)
C136	6779.9(19)	2602(8)	5862.6(12)
C135	7029(2)	2932(11)	6029.7(18)
C134	7012(4)	3540(10)	6095(3)
C133	6746(4)	3817(8)	5994(4)
C132	6497(3)	3486(6)	5827(3)
C131	6514(2)	2879(6)	5761.4(16)
C141	5681(7)	1519(17)	5934(7)
C140	5858(7)	1625(17)	6232(6)
C139	6111(7)	1953(16)	6323(4)
C138	6185(7)	2175(18)	6117(3)
C137	6007(6)	2069(16)	5819(4)
C142	5755(5)	1741(14)	5728(5)
C143	5447(7)	3952(15)	4988(8)
C144	5440(8)	3874(17)	5189(9)
C145	5110(6)	4746(12)	5017(3)
F49	4236(9)	634(18)	2555(8)
F50	4469(8)	-89(19)	2900(8)
F51	4359(8)	758(18)	2976(8)
F52	5486(7)	26(9)	3538(6)
F53	5573(7)	930(11)	3651(5)
F54	5723(4)	525(14)	3390(6)
F57A	5808(10)	2771(11)	2301(7)
F58A	6091(4)	3380(20)	2637(10)
F59A	5651(9)	3695(13)	2258(7)
C213	4952(4)	536(13)	3092(5)
C214	5219(3)	776(15)	3159(5)
C215	5241(5)	1240(15)	2988(7)
C210	4996(7)	1466(14)	2749(7)
C211	4729(5)	1226(16)	2682(6)
C212	4707(3)	762(15)	2853(6)
C216	5488(3)	563(9)	3420(4)
C217	4436(5)	480(20)	2820(11)
C221	5720(3)	3317(6)	2895(3)
F1G	5464(5)	3875(9)	3299(4)
F55	5613(5)	3005(10)	3522(4)
F56	5914(4)	3625(9)	3483(3)
F57	5645(5)	3217(12)	2164(3)
F58	6048(4)	2924(12)	2532(4)
F59	5896(5)	3852(10)	2518(4)
C218	5311(5)	2388(10)	2662(5)
C219	5376(4)	2644(9)	2934(4)

C220	5581(3)	3108(7)	3050(3)
C222	5652(3)	3059(8)	2622(3)
C223	5448(4)	2593(9)	2506(4)
C224	5644(4)	3401(8)	3338(3)
C225	5809(4)	3265(10)	2459(4)
B3	5000	2070(60)	2500

Computational Methodology

Variational two-electron reduced density matrix (V2RDM) calculations were performed using the Maple Quantum Chemistry Package (QCP).[8] Natural orbital density plots were obtained using the DensityPlot3D procedure in QCP. As with wave-function-based complete active-space self-consistent-field (CASSCF) techniques, active-space V2RDM variationally solves the Schrödinger equation for an active set of orbitals, known as an active space, followed by orbital rotations between the active and inactive orbitals to lower the energy until self-consistency is achieved.[9] V2RDM has been successfully used to account for most of the strong correlation in a variety of large transition-metal molecules.[10] The major advantage of V2RDM over traditional wave-function-based methods is its favorable polynomial scaling of $O(r^6)$, compared to the $O(r^N)$ exponential scaling of conventional wave-function-based methods (where r is the number of basis functions and N is the number of active electrons). This scaling is the result of the fact that in V2RDM calculations the 2-RDM is computed directly, avoiding the explicit calculation of the entire wave function.

As fermionic interactions are pairwise the energy of any system can be expressed as a linear functional of the 2-RDM: $E = Tr[{}^2K\,{}^2D]$, where ${}^2K$ is the 2-electron reduced Hamiltonian, and ${}^2D$ is the 2-RDM. The energy is variationally minimized using a semidefinite program,[11] which minimizes the energy as a functional of the 2-RDM subject to several N-representability constraints:[12]

$$ {}^2D \succeq 0 \tag{1} $$

$$ {}^2Q \succeq 0 \tag{2} $$

$$ {}^2G \succeq 0 \tag{3} $$

These conditions are termed the DQG conditions, where ${}^2D$ is the two-particle matrix, ${}^2Q$ is the two-hole matrix, ${}^2G$ the particle-hole matrix, and $M \succeq 0$ indicates that matrix M is positive semidefinite, meaning its eigenvalues are nonnegative. As the 2-RDM is calculated directly, without the wave function, the DQG conditions are necessary to ensure that the 2-RDM remains N-representable, meaning there must be a corresponding N-electron wave function. The minimized energy from a V2RDM calculation represents a lower bound to the true ground state energy. Calculations using [19,20] active spaces as carried out in this in study remain outside the scope of traditional wave-function-based CASSCF methods.

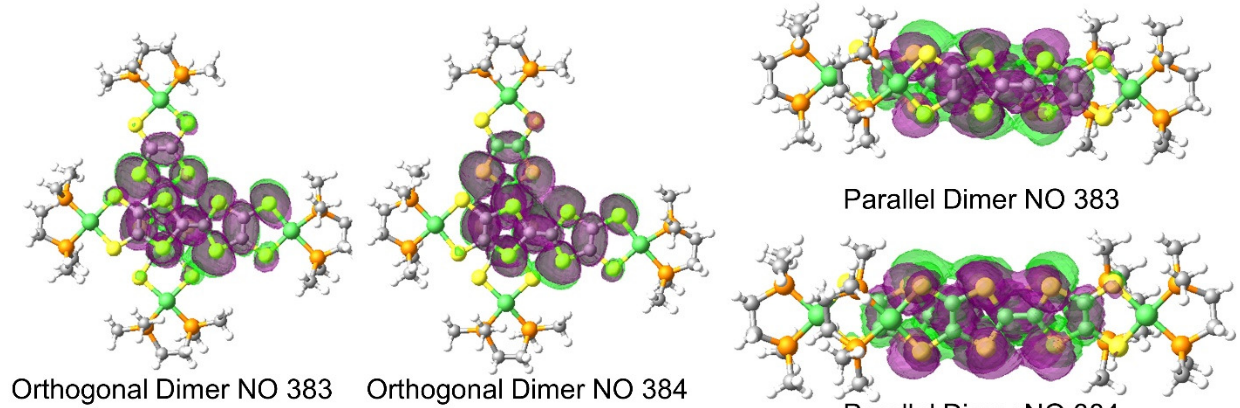

Orthogonal Dimer NO 383 Orthogonal Dimer NO 384

Parallel Dimer NO 383

Parallel Dimer NO 384

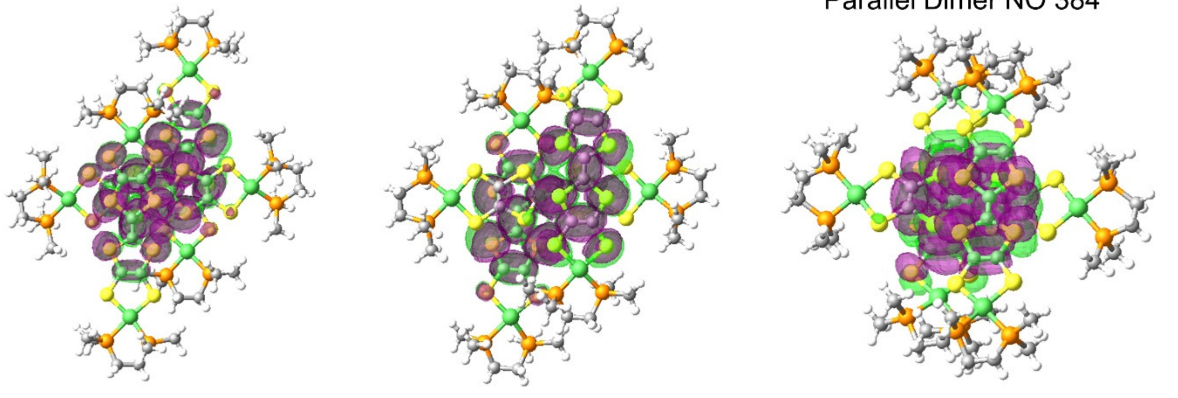

Trimer NO 574 Trimer NO 575 Trimer NO 576

Figure S59. Orbital density plots for the computationally treated dimers and trimers viewed along the stacking interaction.

Table S7. Energies, NO occupations and Mulliken charges for the two different dimerization geometries. V2RDM calculations with a [19,20] active space and 3-21G basis set.

	Parallel	Orthogonal
E(a.u.)	-16430.761095	-16430.712292
$\lambda 382$	1.88571	1.912486
$\lambda 383$	1.49923	1.224860
$\lambda 384$	0.51331	0.771141
$\lambda 385$	0.08481	0.073175
$q1$	0.40607	0.37830
$q2$	0.56836	0.43482
$q3$	0.57037	0.45403
$q4$	0.40265	0.43870

Table S8. Energies, NO occupations and Ni atom Mulliken charges for the trimer unit. V2RDM calculations were performed with a [17,20] active space and 3-21G basis set.

	V2RDM
E(a.u.)	-24645.905214
λ573	1.92977
λ574	1.32748
λ575	0.97218
λ576	0.64935
λ577	0.06524
q1	0.44168
q2	0.44892
q3	0.43547
q4	0.43356
q5	0.44406
q6	0.43699

Cited References

[1] Svenstrup, N.; Rasmussen, K. M.; Hansen, T. K.; Becher, J. The Chemistry of TTFTT; 1: New Efficient Synthesis and Reactions of Tetrathiafulvalene-2,3,6,7-Tetrathiolate (TTFTT): An Important Building Block in TTF-Syntheses. *Synthesis.* **1994**, 809–812.

[2] (a)Van Hecke, G. R.; Horrocks, W. D. Ditertiary Phosphine Complexes of Nickel. SpeCtral, Magnetic, and Proton Resonance Studies. A Planar-Tetrahedral Equilibrium. *Inorg. Chem.* **1966**, *5* (11), 1968–1974. (b)Angulo, I. M.; Bouwman, E.; van Gorkum, R.; Lok, S. M.; Lutz, M.; Spek, A. L. New Nickel-Containing Homogeneous Hydrogenation Catalysts. *J. Mol. Catal. A Chem.* **2003**, *202* (1–2), 97–106.

[3] Chávez, I.; Alvarez-Carena, A.; Molins*, E.; Roig, A.; Maniukiewicz, W.; Arancibia, A.; Arancibia, V.; Brand, H.; Manuel Manríquez*, J. Selective Oxidants for Organometallic Compounds Containing a Stabilising Anion of Highly Reactive Cations: $(3,5(CF_3)_2C_6H_3)_4B^-)Cp_2Fe^+$ and $(3,5(CF_3)_2C_6H_3)_4B^-)Cp^*{}_2Fe^+$. *J. Organomet. Chem.* **2000**, *601* (1), 126–132.

[4] Hunter, B. K.; Reeves, L. W. Chemical Shifts for Compounds of the Group IV Elements Silicon and Tin *Can. J. Chem.* **1968**, *46*, 1399-1414.

[5] Sheldrick, G. M. SHELXT- Integrated space-group and crystal-structure determination. *Acta Cryst***.** **2015**, *A71*, 3- 9

[6] Dolomanov, O.V.; Bourhis, L. J.; Gildea, R. J.; Howard, A. K.; and Puschmann, H., Olex2, a complete structure solution, refinement, and analysis program. *J. Appl. Cryst*. **2009**. *42*, 339

[7] (a) Sheldrick, G. M. A Short History of SHELX. *Acta Cryst*. **2008***, A64*, 112-122; (b) Sheldrick, G. M. Crystal structure refinement with SHELXL. *Acta Cryst*. **2015,** *C71*, 3-8

[8] Maple Quantum Chemistry Toolbox (**2019**). Maplesoft, a division of Waterloo Maple Inc., Waterloo, Ontario.

[9] (a) Mazziotti, D. A. Two-Electron Reduced Density Matrix as the Basic Variable in Many-Electron Quantum Chemistry and Physics. *Chem. Rev.* **2012**, 112, 244−262. (b) Mazziotti, D. A., Ed. Variational Two-Electron Reduced-Density Matrix Theory. In Reduced-Density-Matrix Mechanics: With Application to Many-Electron Atoms and Molecules; John Wiley and Sons, Inc.: Hoboken, NJ, **2007**; pp 19−59. (c) Nakata, M.; Nakatsuji, H.; Ehara, M.; Fukuda, M.; Nakata, K.; Fujisawa, K. Variational Calculations of Fermion Second-Order Reduced Density Matrices by Semidefinite Programming Algorithm. *J. Chem. Phys.* **2001**, 114, 8282−8292. (d) Mazziotti, D. Realization of Quantum Chemistry without Wave Functions through First-Order Semidefinite

Programming. *Phys. Rev. Lett.* **2004**, 93, 213001. (e) Gidofalvi, G. and Mazziotti, D. A. Active-Space Two-Electron Reduced-Density-Matrix Method: Complete Active-Space Calculations without Diagonalization of the N-electron Hamiltonian. *J. Chem. Phys.* **2008**, 129, 134108. (f) Shenvi, N.; Izmaylov, A. F. Active-Space N-Representability Constraints for Variational Two-Particle Reduced Density Matrix Calculations. *Phys. Rev. Lett.* **2010**, 105, 213003. (g) Verstichel, B.; van Aggelen, H.; Poelmans, W.; Van Neck, D. Variational Two-Particle Density Matrix Calculation for the Hubbard Model Below Half Filling Using Spin-Adapted Lifting Conditions. *Phys. Rev. Lett.* **2012**, 108, 213001. (h) Fosso-Tande, J.; Nguyen, T.-S.; Gidofalvi, G.; DePrince, A. E., III Large-Scale Variational Two-Electron Reduced-Density-Matrix Driven Complete Active Space Self-Consistent Field Methods. *J. Chem. Theory Comput.* **2016**, 12, 2260−2271. (i) Mazziotti, D. A. Enhanced Constraints for Accurate Lower Bounds on Many-Electron Quantum Energies from Variational Two Electron Reduced Density Matrix Theory. *Phys. Rev. Lett.* **2016**, 117, 153001.

[10] (a) Schlimgen, A. W.; Heaps, C. W.; Mazziotti, D. A. Entangled Electrons Foil Synthesis of Elusive Low-Valent Vanadium Oxo Complex. *J. Phys. Chem. Lett* **2016**, 7, 627–631. (b) Schlimgen, A. W.; Mazziotti, D. A. Static and Dynamic Electron Correlation in the Ligand Noninnocent Oxidation of Nickel Dithiolates. *J. Phys. Chem. A* **2017**, 121, 9377–9384. (c) Montgomery, J. M.; Mazziotti, D. A. Strong Electron Correlation in Nitrogenase Cofactor, FeMoco. *J. Phys. Chem. A* **2018**, 122, 4988–4996. (d) McIsaac, A. R.; Mazziotti, D. A. Ligand Non-innocence and Strong Correlation in Manganese Superoxide Dismutase Mimics. Phys. Chem. Chem. Phys. **2017**,19, 4656–4660.

[11] (a) Mazziotti, D. A. First-order Semidefinite Programming for the Two-electron Treatment of Many-Electron Atoms and Molecules. *ESAIM: Math. Modell. Numer. Anal.* **2007**, 41, 249−259. (b) Mazziotti, D. A. Large-Scale Semidefinite Programming for Many-Electron Quantum Mechanics. *Phys. Rev. Lett.* **2011**, 106, 083001.

[12] (a) Mazziotti, D. A. Variational reduced-density-matrix method using three-particle *N*-representability conditions with application to many-electron molecules. *Phys. Rev. A: At., Mol., Opt. Phys.* **2006**, 74, 032501. (b) Garrod C. and Percus, J. Reduction of the *N*-Particle Variational Problem. J. Math. Phys. (N.Y.) **1964**, 5, 1756.